Lithos 224–225 (2015) 310–323

Contents lists available at ScienceDirect

Lithos

journal homepage: www.elsevier.com/locate/lithos

Hydrothermal alteration and melting of the crust during the Columbia River Basalt–Snake River Plain transition and the origin of low-$\delta^{18}O$ rhyolites of the central Snake River Plain

Dylan P. Colón [a,*], Ilya N. Bindeman [a], Ben S. Ellis [b], Axel K. Schmitt [c], Christopher M. Fisher [d]

[a] Department of Geology, University of Oregon, Eugene, OR, USA
[b] Institute of Geochemistry and Petrology, Eidgenössische Technische Hochschule Zürich, Zürich, Switzerland
[c] Department of Earth, Planetary, and Space Sciences, University of California Los Angeles, Los Angeles, CA, USA
[d] School of the Environment, Washington State University, Pullman, WA, USA

ARTICLE INFO

Article history:
Received 1 December 2014
Accepted 22 February 2015
Available online 4 March 2015

Keywords:
Isotopes
Snake River Plain
Zircon
Rhyolite
Hydrothermal alteration

ABSTRACT

We present compelling isotopic evidence from ~15 Ma rhyolites that erupted coeval with the Columbia River Basalts in southwest Idaho's J-P Desert and the Jarbidge Mountains of northern Nevada at that suggests that the Yellowstone mantle plume caused hydrothermal alteration and remelting of diverse compositions of shallow crust in the area where they erupted. These rhyolites also constitute the earliest known Miocene volcanism in the vicinity of the Bruneau–Jarbidge and Twin Falls (BJTF) volcanic complexes, a major center of voluminous (10^3–10^4 km^3) low-$\delta^{18}O$ rhyolitic volcanism that was previously defined as being active from 13 to 6 Ma. The Jarbidge Rhyolite has above-mantle $\delta^{18}O$ ($\delta^{18}O$ of +7.9‰ SMOW) and extremely unradiogenic ε_{Hf} (−34.7) and ε_{Nd} (−24.0). By contrast, the J-P Desert units are lower in $\delta^{18}O$ (+4.5 to 5.8‰), and have more moderately unradiogenic whole-rock ε_{Hf} (−20.3 to −8.9) and ε_{Nd} (−13.4 to −7.7). The J-P Desert rhyolites are geochemically and petrologically similar to the younger rhyolites of the BJTF center (the one exception being their high $\delta^{18}O$ values), suggesting a common origin for J-P Desert and BJTF rhyolites. The presence of low-$\delta^{18}O$ values and unradiogenic Nd and Hf isotopic compositions, both of which differ greatly from the composition of a mantle differentiate, indicate that some of these melts may be 50% or more melted crust by volume. Individual J-P Desert units have isotopically diverse zircons, with one lava containing zircons ranging from −0.6‰ to +6.5‰ in $\delta^{18}O$ and from −29.5 to −2.8 in ε_{Hf}. Despite this diversity, zircons all have Miocene U/Pb ages. The range of zircon compositions fingerprints the diversity of their source melts, which in turn allow us to determine the compositions of two crustal end-members which melted to form these rhyolites. These end-members are: 1) Archean basement with normal to high-$\delta^{18}O$ and unradiogenic ε_{Hf} and 2) hydrothermally altered, shallow, young crust with low-$\delta^{18}O$ (0–1‰) and more radiogenic ε_{Hf}. We suggest that the shallow crust's low-$\delta^{18}O$ composition is the result of hydrothermal alteration which was driven by a combination of normal faulting and high heat fluxes from intruding Yellowstone plume-derived basalts shortly prior to the onset of silicic magmatism. Furthermore, zircon diversity in the J-P Desert units suggests rapid assembly of zircon-bearing melts of varying isotopic composition prior to eruption, creating well-mixed magmas with heterogeneous zircons. We suggest that this hydrothermal priming of the crust followed by remelting upon further heating may be a common feature of intraplate mantle plume volcanism worldwide.

1. Introduction

The time transgressive series of eruptive centers along the Yellowstone hotspot track connects the modern eruptive center at the Yellowstone Plateau with the ~16 Ma Columbia River flood basalts (CRBs) (e.g., Pierce and Morgan, 1992). The flood basalts and their associated silicic magmatism, together with the younger hotspot track, are most commonly interpreted as the expression of a deep-sourced mantle plume (Camp and Ross, 2004; Schmandt et al., 2012), though other interpretations are also discussed (Carlson, 1984; Christiansen et al., 2002; Liu and Stegman, 2012). Unlike the focused silicic centers that characterize past and present activity along the hotspot track of the Snake River Plain (SRP) and Yellowstone, the syn-CRB silicic volcanism occurred nearly simultaneously over a roughly circular region at least 400 km across which is presumed to have been underlain by the head of the Yellowstone plume (Fig. 1) (Camp and Ross, 2004; Coble and Mahood, 2012; Ferns and McClaughry, 2013).

* Corresponding author at: Department of Geology, 1272 University of Oregon, Eugene, OR 97403-1272, USA. Tel.: +1 608 630 4700.
E-mail address: dcolon@uoregon.edu (D.P. Colón).

http://dx.doi.org/10.1016/j.lithos.2015.02.022
0024-4937/

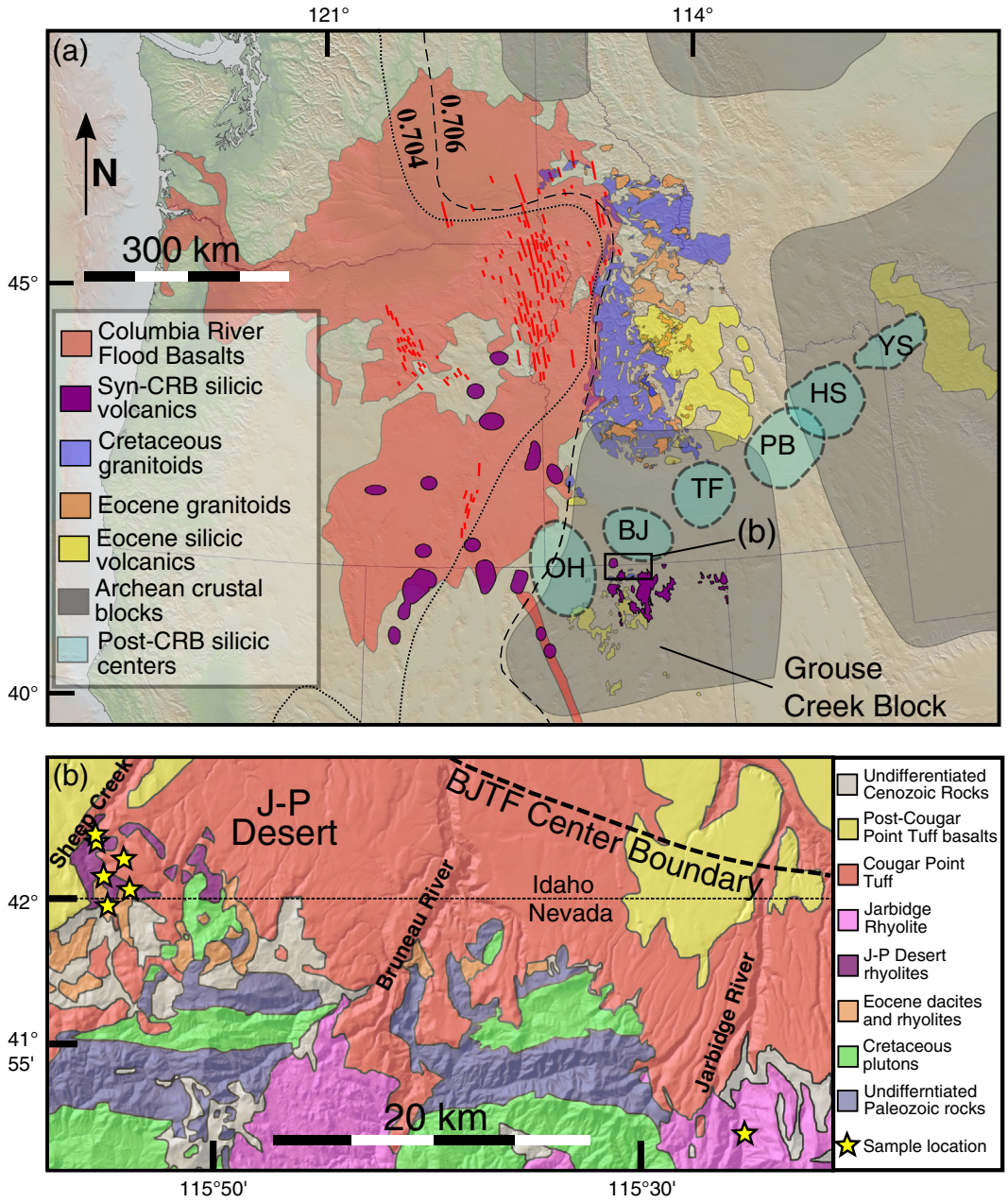

Fig. 1. Regional and local maps of the study area. (a) Extent of volcanism due to the Yellowstone Plume at 14.5–17 Ma. Red areas show the region covered by the CRBs (including the Northern Nevada Rift), which erupted from 17 to 15.5 Ma (Camp and Ross, 2004; Reidel et al., 2013; Wolff et al., 2008). Dike swarms that fed the flood basalt eruptions are shown in dark red (Camp and Ross, 2004). Syn-CRB rhyolites of age 14.5 Ma and older are shown in pink (Coats, 1987; Coble and Mahood, 2012; Ferns and McClaughry, 2013; Steiner and Streck, 2013; Streck et al., 2011). Mapped centers of rhyolitic volcanism are not exhaustive, but show all centers estimated as having at least 20 km^3 of rhyolite by Coble and Mahood (2012, Supplementary material). Large inferred or observed volcanic centers that occurred along the Yellowstone hotspot track from 14.5 Ma to the present are indicated by dotted lines. These include the Owyhee–Humboldt–Juniper Mountain (OH), Bruneau–Jarbidge (BJ), Twin Falls (TF), Picabo (PB), Heise (HS), and Yellowstone (YS) centers (Bonnichsen et al., 2008; Drew et al., 2013). All of these large post 14.5 Ma caldera centers have been host to low-$\delta^{18}O$ volcanism. Additional mapped features include the Archean crustal blocks of Foster et al. (gray) (2006), locations of Eocene volcanism of the Challis and Absaroka volcanics (yellow) (Norman and Mertzman, 1991), Cretaceous and Eocene intrusives of the Idaho batholith, Challis intrusives, and adjacent areas (Boroughs et al., 2012; Coats, 1987; Gaschnig et al., 2011). (b) Detail of the study area, simplified from Bernt and Bonnichsen (1982), Coats (1987), and Link (2002). Dashed edge of the ~13–11 Ma Bruneau–Jarbidge volcanic complex is taken from Bonnichsen et al. (2008). Stars show sample locations (Table 1). Bases for both maps obtained from the Global Multi-Resolution Topography (GMRT) synthesis (GeoMapApp.org). Small outcrops of Seventy Six basalt are located south of the map area. (For interpretation of the references to color in this figure legend, the reader is referred to the web version of this article.)

In this study we investigate a group of rhyolites in the J-P Desert of Idaho, which is defined as the area between Sheep Creek and the Bruneau River in Owyhee County, southwest Idaho, and compare them to one sample of the Jarbidge Rhyolite 45 km southwest of the J-P Desert locality in northern Nevada (Fig. 1b). This places them on the geographic boundary between the broad unfocused silicic volcanism that accompanied the CRBs and the more focused silicic volcanism that characterizes the volcanic centers of the SRP. Additionally, these units are overlain by ashflow tuffs identified as belonging to the Bruneau–Jarbidge volcanic center, the oldest of the major eruptive centers of the Snake River Plain (Bernt and Bonnichsen, 1982; Bonnichsen et al., 2008), making them also temporally intermediate between the

majority of the SRP rhyolites and the older CRB related rhyolites. This allows us to group the J-P Desert rhyolites with both the Columbia River Basalt-age rhyolites and the Snake River Plain hotspot track rhyolites, and identify them as transitional between the two. Investigating the timing and origins of the J-P Desert volcanism is therefore crucial to reconstructing the conditions governing the transition between these two mantle plume-driven volcanic regimes. In this study we combine U–Pb geochronology and analyses of Hf, Nd, and O isotopes and trace elements in whole rocks and mineral separates to determine ages and to distinguish sources of the J-P Desert and Jarbidge rhyolite magmas to better constrain the magma-tectonic interactions that produced them.

2. J-P Desert stratigraphy and sampling

The Miocene silicic tuffs and lavas of the southern J-P Desert in southwest Idaho outcrop on top of older ~50 Ma Eocene calc-alkaline andesites and dacites of the Bieroth volcanics, which were named and mapped by Bernt and Bonnichsen (1982) (Fig. 1b). The welded ignimbrite called the Rough Mountain Rhyolite is the oldest Miocene unit of the J-P Desert suite, outcropping directly above Eocene Bieroth volcanics (see Supplementary material for photographs). It is more than 170 m thick in places, and has been interpreted as a caldera infill deposit on the basis of its thickness (Bernt and Bonnichsen, 1982), although we note that distinguishing between strongly welded ignimbrites and rhyolitic lavas in the SRP remains difficult (e.g., Branney et al., 2008). The overlying Lapilli Tuff of Sheep Creek is up to 40 m thick, well-bedded, and unwelded. It was interpreted as a near-vent fallout deposit (Bernt and Bonnichsen, 1982). The Johnstons Camp Rhyolite comprises a series of lava flows over 60 m thick that also lies above the Rough Mountain Rhyolite, but these lava flows are of uncertain stratigraphic relationship with the Lapilli Tuff of Sheep Creek (Bernt and Bonnichsen, 1982). Other younger Miocene units in the area include the Whiskey Draw Rhyolite, the Tuff of Browns Basin, and the Rattlesnake Draw Tuff (Fig. 1b). Most if not all of these rocks have experienced substantial post-emplacement hydrothermal alteration, evident from silicification and the growth of secondary minerals. Lying on top of these ~15 Ma units is the ~13–10 Ma Cougar Point Tuff succession originating from the Bruneau–Jarbidge volcanic center of the central SRP just to the north, which we suggest is a continuation of the J-P Desert volcanism. Volcanism at Bruneau–Jarbidge was followed by activity Twin Falls complex (Fig. 1a), with no significant pause in volcanism during the 13–8 Ma duration of both centers (Bonnichsen et al., 2008). From this, and their similar isotopic character (discussed below), we group them together for the remainder of this paper as a single volcanic field (BJTF). The volcanic relicts which are preserved in the J-P Desert were also coeval with eruptions of the ~16.1–15.0 Ma Jarbidge Rhyolite 50 km to the southeast in northern Nevada, which consists of several voluminous lavas totaling up to 500 km^3 that erupted over a ~60 km × 30 km area (Fig. 1a) (Brueseke et al., 2014). We analyzed in detail one sample of the main body of the Jarbidge Rhyolite collected just south of the town of Jarbidge, Nevada.

3. Analytical methods

Zircon crystals were extracted from four units (Table 2, Fig. 1) via bulk dissolution of ~100 g of each sample in cold 48% hydrofluoric acid for two to three days following the extraction protocol in Bindeman (2003, Appendix), which is the preferred method for crystal-poor altered volcanic rocks. Because zircon is not readily soluble in cold HF, it is then easy to extract from the resulting residue via either direct picking or density separation. The use of separate containers during digestion minimizes the potential for cross-sample zircon contamination. Hand-picked zircons were mounted in epoxy, sectioned by grinding with abrasives (SiC and diamond), and cleaned and coated with a conductive Au layer for isotope analysis.

Zircon $\delta^{18}O$ and U–Pb analyses were conducted using the CAMECA IMS 1270 at the University of California-Los Angeles. Instrumental bias was corrected by interspersed analyses of AS3 standard zircon (1099.1 Ma; Paces and Miller, 1993; $\delta^{18}O = 5.3‰$ SMOW; Trail et al., 2007) mounted in close physical proximity to the unknowns. External reproducibility of the AS3 standards was 1.6% (n = 14) for $^{206}Pb/^{238}U$ and 0.20‰ (1 s.d.) for $\delta^{18}O$; accuracy was tested by standard intercalibration using zircon 91500 (Wiedenbeck et al., 2004), which was found to be within the stated analytical uncertainties for $^{206}Pb/^{238}U$ and $\delta^{18}O$. The $\delta^{18}O$ ($^{133}Cs^+$ beam) and U–Pb age (^{16}O beam) analyses were performed in sequential analytical session overlapping ~30 μm spots (the second directly on top of a pre-existing pit), which were then confirmed to be in zircon cores by cathodoluminescence images obtained at the University of Oregon.

Zircons were then repolished and laser ablation analysis spots ~30 μm in diameter for ε_{Hf} were placed in close to locations for $\delta^{18}O$ and U–Pb analyses. Zircon ε_{Hf} analyses were performed with a ThermoFinnigan Neptune multi-collector inductively-coupled plasma mass-spectrometer (LA-MC-ICPMS) at Washington State University, following the method of Fisher et al. (2014) using Plešovice zircon standard with a $^{176}Hf/^{177}Hf$ ratio of 0.282482 (Sláma et al., 2008) (measured at 0.282439 and corrected accordingly). It should be noted that LA-ICP-MS spots, while of approximately the same diameter as ion microprobe spots, sample a much larger volume of zircon.

Whole rock powders from the same samples were used to determine the bulk Hf and Nd isotopic compositions using the Neptune MC-ICPMS at WSU, following the methods of Gaschnig et al. (2011) and using standards of JMC 475 ($^{176}Hf/^{177}Hf = 0.282160$) with a reproducibility of ±0.000005 (2 s.d.) and LaJolla ($^{143}Nd/^{144}Nd = 0.511858$) with a reproducibility of 0.000011 (2 s.d.). Whole rock samples of the J-P Desert units were carefully crushed and powdered using standard techniques at the GeoAnalytical Laboratory in Washington State University. Low-dilution, doubly fused glass beads were then made for analysis of major and trace elements with a ThermoARL Advant XP for major and trace elements via X-ray fluorescence and an Agilent 7700 ICP-MS for traces and rare earth elements. The Jarbidge Rhyolite was analyzed for major and trace elements via X-ray fluorescence at Ponoma College.

Additional spot analyses of zircon for Ti and other trace elements were performed at the Eidgenössische Technische Hochschule (ETH) Zürich using a 193 nm Resonetics ArF excimer laser coupled to a Thermo Element XR ICPMS within the Institute of Geochemistry and Petrology. Spot sizes were 30 μm and the output energy of the laser beam was typically 3.5 J/cm^2. NIST 612 was used as the primary standard and two secondary standards, the GSD-1G glass and GJ-1 zircon, were used to monitor data quality. All trace elemental data from zircons were reduced using the ETH-developed SILLS program (Guillong et al., 2008). Trace elemental abundances are considered to have a precision of <5%.

Phenocrysts of quartz and feldspar for oxygen isotope measurements were obtained after careful petrographic examination of crystals under a binocular microscope. As all collected units were weathered and secondarily silicified, particular care was devoted to identifying primary magmatic phenocrysts, which are typically equant, as opposed to secondary minerals, which are often singly terminated or irregular in appearance. The presence of (volumetrically insignificant) melt inclusions was used as an additional guiding principle in selecting magmatic crystals. Crystals also had residual glass cleaned off of them via a wash in cold HF for 1–2 h. Oxygen isotopic compositions (reported as $\delta^{18}O$ SMOW) of major phenocrysts (quartz and plagioclase) were measured via an integrated laser fluorination-MAT-253 mass spectrometer system at the University of Oregon (Bindeman, 2008), using BrF_5 as the fluorinating reagent. Samples were controlled for reproducibility via intercalibration with a UOG (6.52‰) garnet standard measured relative to a Gore Mountain Garnet standard of 5.8‰ (Valley et al., 1995). Errors on repeat measurements of standards are typically better than 0.2‰ (2 s.d.).

4. Results

4.1. U–Pb geochronology

Weighted mean $^{238}U/^{206}Pb$ ages with 2σ uncertainties from zircon SIMS spot analyses (Fig. 2, Table 2) are 14.7 ± 0.37 Ma (n = 14 used out of 14 total ages) for the Johnstons Camp Rhyolite, 14.6 ± 0.42 Ma (n = 10 of 10) for the Lapilli Tuff of Sheep Creek, 15.3 ± 0.38 Ma (n = 10 of 11) for the Rough Mountain Rhyolite, and 15.3 ± 0.66 Ma (n = 6 of 9) for the Jarbidge Rhyolite. For the Jarbidge Rhyolite, three older crystals with ages up to 18.9 ± 1.8 Ma (xenocrysts or antecrysts) were excluded until the MSWD met the criterion for a single population at the 95% confidence level as tabulated in Mahon (1996), in order to isolate the youngest zircon age population. The 15.3 Ma zircon age is in good agreement with a 15.30 ± 0.18 $^{40}Ar/^{39}Ar$ age reported by Brueseke et al. (2014) for sanidine from Jarbidge Rhyolite outcropping near our sampling site. Although their errors overlap, the age progression is consistent with the observed stratigraphy of the J-P Desert units.

4.2. Major phenocryst O isotopes and whole rock Hf and Nd isotopes

Nearly all major phenocryst $\delta^{18}O$ values from J-P Desert or Jarbidge rhyolites (Fig. 4, Table 1) fall within 2‰ of the "normal" quartz $\delta^{18}O$ ($\delta^{18}O_{qz}$) value of ~+6.5‰ SMOW for quartz, the "normal" plagioclase $\delta^{18}O$ ($\delta^{18}O_{plag}$) of ~+5.0 to 5.8‰ (depending on Ca content of plagioclase), or their equivalents for other minerals expected for a 900 °C rhyolitic differentiate of a mantle-derived basalt (Chiba et al., 1989; Bindeman, 2008). Magmatic quartz phenocrysts from the Jarbidge Rhyolite sample have an above-normal $\delta^{18}O_{qz}$ value of +8.4‰, similar to other $\delta^{18}O_{qz}$ values of Jarbidge Rhyolite reported in Brueseke et al. (2014). In contrast, quartz grains from the Rough Mountain Rhyolite and the Lapilli Tuff of Sheep Creek have slightly below normal $\delta^{18}O_{qz}$ values, of +5.0‰ and +5.2‰, respectively. The sample of Johnstons Camp Rhyolite was quartz-undersaturated but produced a reliably reproduced $\delta^{18}O_{plag}$ value of +5.8‰. By contrast, a sample of the Cedar Creek Tuff member of the Eocene Bieroth volcanics has $\delta^{18}O_{qz}$ as high as +9.5‰. We also measured the $\delta^{18}O_{plag}$ of the lowest exposed member of the younger Cougar Point Tuff sequence of the BJTF complex at +1.3‰ (Table 1).

The hafnium and neodymium isotopic compositions of bulk rock samples (Fig. 3, Table 1) are all unradiogenic when compared to chondrite universal reservoir (ε_{Nd} and $\varepsilon_{Hf} = 0$), ranging from ε_{Nd} of −7.7 and ε_{Hf} of −8.9 for the Rough Mountain Rhyolite to ε_{Hf} of −34.7 and ε_{Nd} of −24.0 for the Jarbidge Rhyolite, the latter in close agreement with the −24.8 ε_{Nd} value reported by Nash et al. (2006). ε_{Nd} and ε_{Hf} values were calculated using the CHUR composition of Bouvier et al. (2008) and the decay constants of DePaolo (1981) and Söderlund et al. (2004). The Johnstons Camp Rhyolite, which has an ε_{Nd} of −13.4 and an ε_{Hf} of −20.3, has a radiogenic isotopic composition which, like its oxygen isotopic composition, is intermediate between the Rough Mountain Rhyolite and Lapilli Tuff of Sheep Creek compositions and that of the Jarbidge Rhyolite.

4.3. Zircon isotopic and trace element compositions

Zircon cores from the Jarbidge Rhyolite were homogeneous in $\delta^{18}O$, clustering around +6‰. In contrast, zircons from the J-P Desert units are diverse in $\delta^{18}O$ values, from low-$\delta^{18}O$ to high $\delta^{18}O$ (−0.6‰ to +6.5‰) (Fig. 5, Table 2). The Rough Mountain Rhyolite and Lapilli Tuff of Sheep Creek zircon core $\delta^{18}O$ values range from +0.5‰ to +3.5‰, and the Johnstons Camp Rhyolite shows still greater diversity in zircon core $\delta^{18}O$ values, ranging from −0.6‰ to +6.5% within a single hand sample. Hf isotope analyses targeting the zircon volume directly underneath the co-registered oxygen isotope and U–Pb geochronology spots also show remarkable variability (ε_{Hf} = −39.0 to 0.8) (Fig. 5, Table A5). The Jarbidge Rhyolite shows a limited, but very unradiogenic range of ε_{Hf} from −35 to −39, mirroring its relative homogeneity in oxygen isotopes. The Rough Mountain Rhyolite and the Lapilli Tuff of Sheep Creek shows greater ε_{Hf} diversity, ranging from $\varepsilon_{Hf} = -1$ to −13, and the Johnstons Camp Rhyolite again had the most diverse zircons, with ε_{Hf} values ranging from −4 to −29. In all J-P Desert rhyolites, zircons with more unradiogenic Hf also tend to have higher $\delta^{18}O$ values (Fig. 5).

Nearly all zircons have Ti concentrations ranging from 5 to 16 ppm (Fig. 6); some analyses were higher, but all zircons with elevated Ti also have either extremely high Fe (100s of ppm) concentrations, which indicate that an iron-titanium oxide inclusion may have been sampled, or anomalous concentrations of other rare-earth elements,

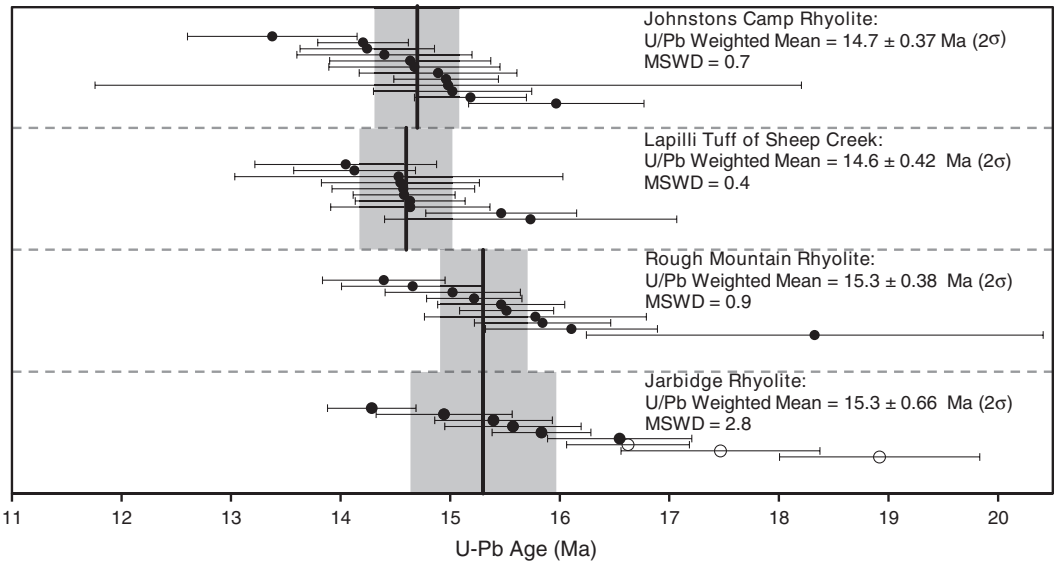

Fig. 2. $^{238}U/^{206}Pb$ ages of J–P Desert rhyolites and the Jarbidge Rhyolite. Points represent individual SIMS spot analyses, with error bars representing 1σ confidence intervals. Zircon ages not used in the mean age calculation for the Jarbidge Rhyolite, which are suspected of being antecrysts, are indicated by open circles. Vertical solid bars are U–Pb weighted mean ages, with shaded areas representing 95% confidence intervals.

Table 1
Whole rock and major phenocryst isotope data.

Unit	Latitude	Longitude	Phenocryst type and $\delta^{18}O$ (‰ SMOW) 2 s.d. = 0.2‰ (major phenocrysts)		Whole rock ε_{Hf}		2 s.e.	Whole rock ε_{Nd}		2 s.e.
Cougar Point Tuff (unit unknown)			Plagioclase (s)	1.32	–		–	–		–
			Plagioclase (s)	0.81						
Whiskey Draw rhyolite	42.00451	−115.91153	Sanidine (s)	4.26	–		–	–		–
			Sanidine (s)	4.37						
Tuff of Browns Basin	41.99738	−115.89178	Plagioclase (s)	3.77	–		–	–		–
			Plagioclase (s)	3.66						
			Plagioclase (m)	3.42						
Johnstons Camp rhyolite	42.02109	−115.89611	Plagioclase (s)	5.85[a]	−20.3	±	0.2	−13.4	±	0.1
			Plagioclase (s)	5.82[a]						
			Plagioclase (m)	5.81						
			Zircon range	−0.57 to 6.47						
Lapilli Tuff of Sheep Creek	42.03422	−115.91649	Quartz (m)	5.22	−10.1	±	0.2	−8.8	±	0.2
			Plagioclase (m)	4.82						
			Plagioclase (s)	4.77						
			Plagioclase (s)	5.25						
			Zircon range	0.46 to 3.52						
Rough Mountain rhyolite	42.03152	−115.91373	Quartz (m)	5.04	−8.9	±	0.2	−7.7	±	0.1
			Plagioclase (s)	2.00[b]						
			Plagioclase (s)	3.92						
			Plagioclase (s)	2.39[b]						
			Plagioclase (m)	4.14						
			Zircon range	0.75 to 2.36						
Jarbidge Rhyolite	41.84789	−115.42917	Quartz (s)	8.44	−34.7	±	0.2	−24.0	±	0.1
			Zircon range	5.55 to 6.53						
Cedar Canyon Tuff	41.98953	−115.91016	Quartz (s)	9.31						
			Quartz (s)	9.47						
			Plagioclase (s)	8.87						
			Plagioclase (s)	8.30						
			Plagioclase	8.54						
			Biotite	5.56						
			Biotite	5.67						

[a] Phenocrysts from a different hand sample than studied zircons.
[b] Phenocrysts have low-$\delta^{18}O$ values due to secondary alteration and do not reflect magmatic compositions.

indicating some other possible contamination. Rare earth element patterns in zircons with diverse isotopic compositions are broadly consistent with those of continental granitoids, as per the discrimination model of Belousova et al. (2002) (data included in Supplementary material). All zircons from the J-P Desert and the Jarbidge Rhyolite have moderate positive Ce and negative Eu anomalies (calculated by comparing measured Eu and Ce to the expected value determined from linear interpolation on a rare earth element plot when normalized to the chondritic abundances of McDonough and Sun, 1995).

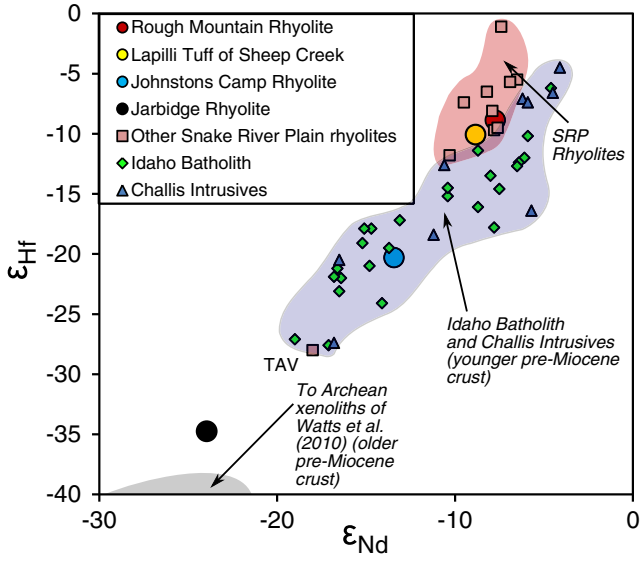

Fig. 3. Whole-rock Hf and Nd isotope values for the Jarbidge Rhyolite and J-P Desert Rhyolites and of other rocks in the region, including Challis intrusives and Idaho Batholith (Gaschnig et al., 2011), and younger Snake River Plain (SRP) rhyolites (Drew et al., 2013; Nash et al., 2006); see Nash et al. (2006) for additional SRP data. All SRP rhyolites fall within a narrow compositional range, with the notable exceptions of the Johnstons Camp rhyolite, and the Tuff of Arbon Valley (TAV), an anomalously unradiogenic rhyolite from the Picabo volcanic center, possibly similar to the Jarbidge Rhyolite in its formation. Two-sigma errors are typically of the size of the data points or smaller (±0.2–0.3 ε units). The "Archean xenolith" field exists outside of the plot area and has an average ε_{Nd} value of −36 (and estimated equivalent ε_{Hf} = −60) from Watts et al. (2010) discussed in the text.

5. Discussion

5.1. Linking J-P Desert and Bruneau–Jarbidge/Twin Falls volcanism

New U–Pb dating of zircons from the J-P Desert and the Jarbidge Rhyolite confirm that the two eruptive centers were active at the same time during the waning period of the Columbia River flood basalt eruptions, which were active primarily from 16.7–15.0 Ma (Reidel et al., 2013), and shortly before the eruption of the oldest previously identified member of the BJTF volcanic complex at ~13 Ma (Bonnichsen et al., 2008). This also makes the J-P Desert and Jarbidge Rhyolites the oldest Miocene rhyolites yet identified in the vicinity of the Central Snake River Plain. The radiogenic isotopic composition of the Rough Mountain Rhyolite is very similar to those of later erupted Bruneau–Jarbidge Cougar Point Tuffs (e.g. ε_{Nd} of −8.2 and ε_{Hf} of −6.5 for the 12.07 Ma Cougar Point Tuff V reported by Nash et al., 2006). Along with very similar major element compositions and mineralogy (Bernt and Bonnichsen, 1982), this suggests that BJTF volcanism was a continuation of the earlier volcanism observed in the J-P Desert.

Perhaps the most convincing link between J-P Desert volcanism and BJTF volcanism, however, is the common presence of low-$\delta^{18}O$ rhyolites at both centers. One of the most enigmatic features of silicic volcanism at Yellowstone and the Snake River Plain in general is the abundance of low-$\delta^{18}O$ rhyolites at all major centers of silicic volcanism (Bindeman and Valley, 2001; Bonnichsen et al., 2008; Boroughs et al., 2005; Drew et al., 2013; Watts et al., 2011). In particular, the rhyolites

Table 2
Zircon $\delta^{18}O$, $^{206}Pb/^{238}U$, and εHf of J–P Desert and Jarbidge Rhyolite zircons. "s.d." is standard deviation.

Unit	Grain #	$\delta^{18}O$ (‰ SMOW)	1 s.d.	$^{206}Pb/^{238}U$ age	1 s.d.	ε_{Hf}	2 s.d.
Jarbidge rhyolite	1	6.24	0.14	15.4	0.5	−35.4	2.6
	2	6.20	0.14	[a]		−37.8	3.2
	3	5.34	0.14	[a]		−36.0	1.1
	4	6.33	0.14	17.5[b]	0.9	−37.1	1.0
	5	6.35	0.14	16.6[b]	0.6	−35.6	1.7
	6	6.12	0.12	18.9[b]	0.9	−36.6	0.9
	7	5.55	0.12	15.8	0.5	−39.0	0.8
	8	5.91	0.12	14.3	0.4	−35.2	0.7
	9	6.3	0.12	14.9	0.6	−36.5	1.0
	10	6.51	0.12	15.6	0.6	−37.8	1.0
	11	6.53	0.12	16.5	0.7	−38.3	2.4
Rough Mountain Rhyolite	1	1.36	0.07	15.8	1	−3.5	1.1
	2	0.90	0.07	15.5	0.6	−4.5	1.2
	3	0.75	0.07	16.1	0.8	−2.4	1.2
	4	1.63	0.07	15.5	0.4	−2.7	0.9
	5	1.87	0.07	14.7	0.7	−9.8	0.9
	6	1.62	0.21	15.2	0.4	−10.2	0.9
	7	2.11	0.21	15.0	0.6	−7.2	0.8
	8	0.55	0.21	18.3	2.1	−0.8	1.8
	9	1.98	0.21	15.8	0.6	−6.5	1.0
	10	2.36	0.21	14.4	0.6	−10.0	0.9
Lapilli Tuff of Sheep Creek	1	3.31	0.17	14.5	0.7	−11.1	1.1
	2	2.91	0.17	14.6	0.7	−11.4	1.2
	3	2.07	0.17	14.6	0.7	−10.8	0.8
	4	2.48	0.17	14.5	1.5	−2.5	0.9
	5	3.50	0.17	14.0	0.8	−12.2	1.1
	6	0.46	0.13	15.5	0.7	−2.4	1.1
	7	2.53	0.13	14.6	0.5	−11.0	0.9
	8	3.52	0.13	15.7	1.3	−13.3	0.8
	9	2.20	0.13	14.6	0.5	−5.3	1.2
	10	2.98	0.13	14.1	0.6	−11.5	1.1
Johnstons Camp Rhyolite	1	5.92	0.16	13.4	0.8	−23.2	1.6
	2	5.46	0.16	14.2	0.4	−21.9	0.9
	3	5.87	0.16	14.7	0.8	−28.1	0.9
	4	2.56	0.16	16.0	0.8	−19.3	4.3
	5	6.02	0.16	14.4	0.8	−28.7	1.4
	6	6.35	0.17	15.0	0.7	−28.1	2.0
	7	6.47	0.17	15.0	3.2	−29.5	1.1
	8	1.23	0.17	14.9	0.7	−2.8	1.1
	9	6.17	0.17	15	0.5	−27.1	0.6
	10 (core)	0.68	0.17	15.9[c]	0.8	−6.2	0.8
	10 (rim)	1.06	0.17	16.8[c]	0.4	−5.0	1.0
	11	−0.57	0.22			−3.9	0.5
	12	2.22	0.22	10.7	15.7	−10.6	1.3
	13	1.06	0.22	15.2	0.5	−15.8	1.7
	14	5.70	0.22	14.6	0.7	−28.3	1.1
	15	5.72	0.22	14.2	0.6	−28.9	0.8

[a] Age discarded due to instrumental error.
[b] Age is good but excluded from weighted average (suspected antecryst).
[c] Age not used in weighted average because of anomalously high U content.

of the BJTF are exclusively low-$\delta^{18}O$ in character (Boroughs et al., 2005, 2012). Most interestingly, however, oxygen isotope data for major phenocryst phases in the J-P Desert, while still below normal values (Table 1), represent perhaps the highest $\delta^{18}O$ values found among Miocene rhyolites in the region, including all BJTF rhyolites (Fig. 4), but excluding normal-$\delta^{18}O$ rhyolites associated with the extension of the Western Snake River Plain (Bonnichsen et al., 2008; Boroughs et al., 2012)

5.2. Linking J-P Desert and Jarbidge Mountains rhyolitic volcanism

The Jarbidge Rhyolite is significantly different from the J-P Desert (and by extension BJTF) rhyolites in its Hf and O isotope composition. Additionally, it appears to be nearly exclusively comprised of lava flows, as opposed to the abundant ash-flow tuffs of the J-P Desert and BJTF (Brueseke et al., 2014). However, rhyolitic eruptions in the Jarbidge Mountains and the J-P Desert were both coeval with other syn-CRB rhyolites in the region (Fig. 1a) and with the waning stages of the CRBs, all of which are likely derived from the impingement of the Yellowstone mantle plume on the base of the crust (Brueseke et al., 2014; Coble and Mahood, 2012; Cummings et al., 2000; Ferns and McClaughry, 2013; Reidel et al., 2013). Regional tectonic extension may have also contributed strongly to magma production in the study area (Fig. 1b), as has been suggested for the Jarbidge Rhyolite by Brueseke et al. (2014), in contrast with BJTF (and the J-P Desert if we indeed group it with BJTF), which is has strong evidence linking it to the mantle plume (Bonnichsen et al., 2008). We argue that this extension was still heavily influenced by the plume, which must have heated and deformed the crust along the margins of its area of impingement (Fig. 1) (e.g. Burov and Guillou-Frottier, 2005). In particular, Brueseke et al. (2014) show via cross-cutting relationships that regional faulting post-dates the Jarbidge Rhyolite yet predates the BJTF succession, suggesting that relaxation of the continental crust associated with extensive crustal melting in Jarbidge-age volcanism may have helped to trigger local faulting, rather than the other way around. Eruptions of the Jarbidge Rhyolite were also coeval with the Seventy Six basalt, minor local eruptions of basalt in the area of the main body of the Jarbidge Rhyolite, that have been dated at 16.5 Ma (Rahl et al., 2002) and are chemically and texturally (plagioclase megaphyric in some outcrops) similar to Steens flood basalts, which are the earliest group of

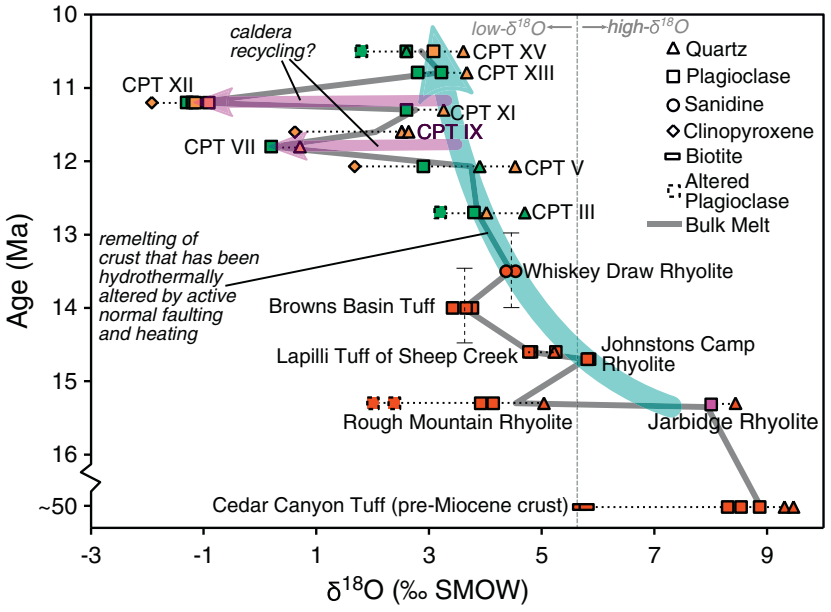

Fig. 4. Plot of $\delta^{18}O$ (‰ SMOW) values for units from this study (red) and measurements of Cougar Point Tuffs of the BJTF center from Boroughs et al. (2005, 2012) (green) and Bindeman and Simakin (2014) (orange). A single plagioclase analysis of Jarbidge Rhyolite (pink) is from Brueseke et al. (2014). Ages are from this study and Bonnichsen et al. (2008). Ages for the Whiskey Draw Rhyolite and the Browns Basin Tuff, are uncertain (error bars) and have been estimated from stratigraphic position. Low-$\delta^{18}O$ plagioclase grains out of equilibrium with quartz are which are suspected of recording secondary rather than magmatic $\delta^{18}O$ are indicated by dashed outlines. A thick gray line shows the evolution of melt $\delta^{18}O$ values with time, estimated by taking either average measured $\delta^{18}O_{qz}$ value minus 0.5‰, or the average $\delta^{18}O_{plag}$ value if there are no available quartz measurements (see Bindeman, 2008). Large shaded arrows illustrate the two processes governing the evolution of oxygen isotopes in these magmas, which result in different trends. These are gradual alteration of the crust through normal faulting, as in Fig. 7, and the recycling of buried and altered intracaldera rhyolites. (For interpretation of the references to color in this figure legend, the reader is referred to the web version of this article.)

CRB lavas to erupt (Camp et al., 2013; Hart and Carlson, 1985). Callicoat (2010) also showed that the trace element composition of the Seventy Six basalt falls within the range defined by the Steens basalts, and concluded based on this result and the textural similarity between the two that the Seventy Six basalt is a member of the Steens basalts. This suggests a common origin for the heating of the crust that produced rhyolites in the Jarbidge Mountains and in the J-P Desert. The strongest evidence, however, for a closely linked relationship between the Jarbidge Rhyolite and the J-P Desert units, to the extent that there may have been a shared magma plumbing system, comes from the Johnstons

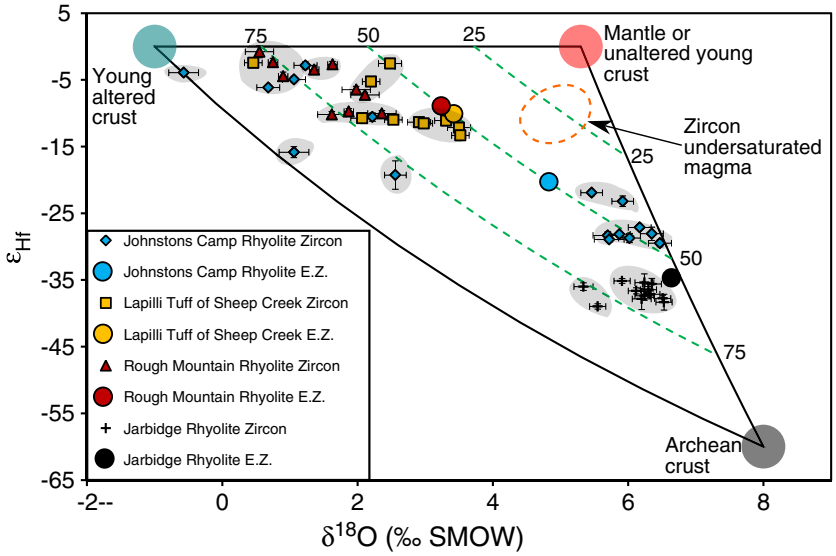

Fig. 5. Hf (ε_{Hf}) and O (‰ SMOW) isotopes in individual zircons of the Jarbidge Rhyolite and the J-P Desert rhyolites relative to isotopic end-members. Diamonds are zircon values. Circles are melt compositions represented by equilibrium zircon $\delta^{18}O$ values from major phenocryst $\delta^{18}O$ (quartz−1.8‰ or, if quartz is absent, plagioclase−1.0‰) measurements coupled with whole-rock Hf isotope measurements (Table 1); error bars are all 1σ. Green dashed lines show minimum contributions of crustal melts of both sources to the erupted magmas. Note that many zircons are derived from magmas that are >75% crustal melts. Gray shaded regions on the plot represent one possible interpretation of the compositions of these magma batches, though the distribution of compositions and there accompanying uncertainty allows significant freedom in choosing possible numbers of batches and their compositions. Also shown is the possible composition of the zircon undersaturated melt that must have mixed with the zircon-bearing melts which contributed to the Rough Mountain Rhyolite and the Lapilli Tuff of Sheep Creek, in order to produce the observed bulk composition given from major phenocrysts. (For interpretation of the references to color in this figure legend, the reader is referred to the web version of this article.)

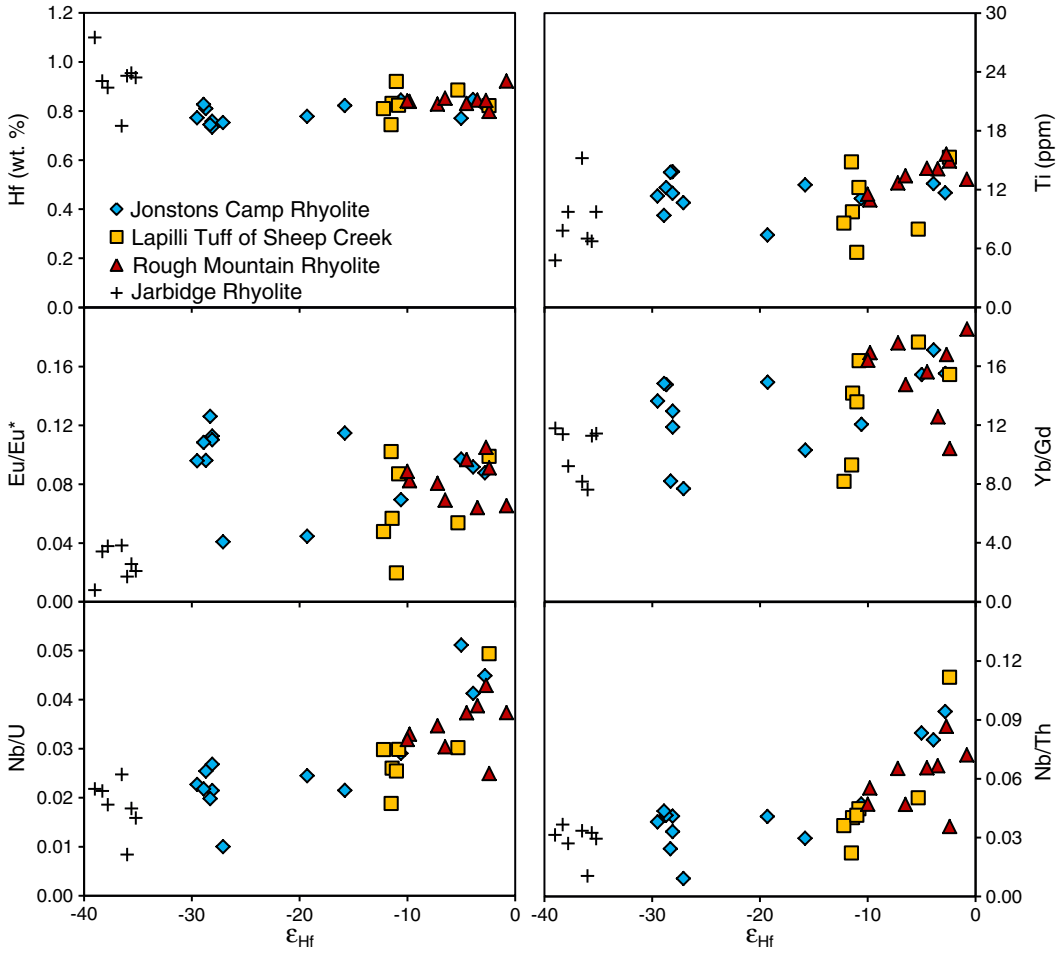

Fig. 6. Trace element compositions (ppm and wt.%) of zircons from the Jarbidge Rhyolite and the J-P Desert rhyolites vs. Hf isotopes (ε_{Hf} units).

Camp Rhyolite in the J-P Desert, which contains zircons that resemble those found in both the Rough Mountain Rhyolite and the Jarbidge Rhyolite in their isotopic and trace element composition (Figs. 5, 6). At a minimum, the magmas that gave rise to the Jarbidge Rhyolite and the some of the Johnstons Camp Rhyolite zircons had similar, if not identical, origins in the crust.

5.3. Origin of extremely unradiogenic Nd and Hf isotope ratios in J-P Desert and Jarbidge magmas

Unradiogenic whole rock and zircon ε_{Hf} and ε_{Nd} values from erupted units in the J-P Desert and from the Jarbidge Rhyolite clearly suggest input of partial melts of ancient Archean crust into erupted magmas (Figs. 3, 5). Archean basement crust has been documented to exist in the area, in the form of the >2.5 Ga Grouse Creek cratonic block (Fig. 1a, Foster et al., 2006). Watts et al. (2010) found an average ε_{Nd} value of −36 for silicic Archean xenoliths from the SRP which, when coupled with the roughly linear relationship observed between Hf and Nd isotopes observed among the J-P Desert and Jarbidge Rhyolite samples, would correspond to an approximate ε_{Hf} value of −60 (Fig. 5). Using the two-stage model of Milisenda et al. (1988) for extraction from depleted mantle, this unradiogenic end member has a Nd model age of 3.2 Ga, if we assume a typical silicic crustal Sm/Nd ratio of 0.18, which is typical of our samples (this is converted to $^{147}Sm/^{144}Nd$ using the isotope abundances of Berglund and Weiser, 2011). We caution that this number almost certainly does not represent the true age of the crustal rocks in the area, and is likely and average of the true age and those of older contaminants (Arndt and Goldstein, 1987), and that the xenoliths from Watts et al. (2010) were not collected in the immediate area of the rhyolites from this study. Along similar lines, we consider obtaining Nd or Hf model ages of the most radiogenic zircons to be impossible because the calculated uncertainties dwarf the ages. Nevertheless the crust which melted to form the Jarbidge Rhyolite is certainly very old. A ~50% mix of a rhyolitic differentiate of the CRBs, which has ε_{Nd} of 0 to +10 (Wolff et al., 2008), and $\varepsilon_{Nd} = -34$ Archean crust is therefore capable of generating magmas with similarly unradiogenic Hf and Nd to the Jarbidge Rhyolite, assuming these end-members have comparable Hf and Nd concentrations. The latter assumption is plausible in the light of minimal differences in Hf concentrations in zircons in different units of the J-P Desert and Jarbidge rhyolites (Fig. 6). Such a high degree of Archean crustal input to a magma is uncommon but not unique to the Jarbidge Rhyolite along the Yellowstone hotspot track; similar rhyolites include the 10.44 Ma Tuff of Arbon Valley, which has ε_{Nd} of −17.7 and ε_{Hf} of −28.0 (and normal $\delta^{18}O$) (Fig. 3) (Drew et al., 2013), and Member C of the Huckleberry Ridge Tuff of Yellowstone, which has an $^{87}Sr/^{86}Sr$ ratio of 0.726 (Doe et al., 1982). Collaborating the unradiogenic ε_{Hf} and ε_{Nd} values in the rocks, Nb/Th and Nb/U ratios, which have been used by Collerson and Kamber (1999) as an indicator of mantle evolution, with larger ratios corresponding to crust derived from younger mantle, show a positive correlation with ε_{Hf} ratios in all zircons (Fig. 6), providing further evidence that zircons with more unradiogenic ε_{Hf} values were derived from melting of older crust. Melting of the Archean crust can only have been accomplished by extensive underplating of middle or upper crustal rocks by intruding basaltic magmas or their silicic differentiates, in volumes far surpassing those of the erupted rhyolites (see below). A

very small amount of this magma may have erupted in the form of the Seventy Six basalt, and if this basalt is indeed related to Steens basalts, it provides further evidence of a link between Jarbidge Rhyolite volcanism and the Yellowstone mantle plume.

5.4. Significance of low-$\delta^{18}O$ magmas

Meteoric water imprints its low-$\delta^{18}O$ oxygen isotopic values on crustal rocks via high-temperature hydrothermal alteration of crustal lithologies in the presence of circulating meteoric waters (Taylor, 1974). This isotope exchange must occur with large water/rock ratios at relatively shallow depths, as deeply penetrating meteoric water can be reasonably expected to lose its low-$\delta^{18}O$ signature via equilibration with shallower high to normal-$\delta^{18}O$ rocks on the way down (Drew et al., 2013; Gottardi et al., 2013; Menzies et al., 2014). Furthermore, these depths are limited by the brittle–ductile transition, which occurs at depths of 5 to 12 km in the Basin and Range province (Gans, 1987), which should serve as a floor for the vast majority of meteoric water circulation in the crust. For J-P Desert, Jarbidge, and BJTF volcanism, we consider the shallow end of that 5–12 km range to be more likely due to the anomalously high geothermal gradient due to the intruding basalts in the area. This is in contrast to the model of Leeman et al. (2008), which suggests an optimal depth of hydrothermal alteration of 15 km. In the absence of pre-existing deep calderas or large throw normal faults which can deeply bury initially shallow protoliths, low-$\delta^{18}O$ volcanism is conclusive evidence of extensive melting of crustal rocks in rhyolite genesis and of the shallow nature of this process.

Intracaldera volcanics, altered by meteoric water in hydrothermal systems analogous to the present day activity at Yellowstone and then deeply buried by the collapse of additional overlapping calderas, have been suggested to be the source of low-$\delta^{18}O$ magmas at Yellowstone and at the Heise and Picabo systems of the East Snake River Plain (Bindeman and Valley, 2001; Drew et al., 2013; Watts et al., 2011, 2012). This means that low-$\delta^{18}O$ rhyolites at these centers are the remelted and "recycled" products of earlier eruptions of the same volcanic center. To be the sole source of low-$\delta^{18}O$ magmas, this mechanism requires that the first eruptive products of a volcanic center have a normal $\delta^{18}O$ composition which is later altered to low values by hydrothermal activity, which is what is observed at the Picabo, Heise, and Yellowstone centers (Bindeman and Valley, 2001; Drew et al., 2013; Watts et al., 2011). In light of this, the origin of voluminous (~10,000 km^3) low-$\delta^{18}O$ rhyolites (Bonnichsen et al., 2008; Boroughs et al., 2005) at the BJTF eruptive center (Fig. 1) that lack exposures of the precursory normal-$\delta^{18}O$ units found at Picabo, Heise, and Yellowstone is less certain and more controversial (Ellis et al., 2013). The search for normal-$\delta^{18}O$ rhyolites in the vicinity of BJTF is therefore of great importance. If no initial normal-$\delta^{18}O$ unit from BJTF can be identified (cf. Watts et al., 2011), then the BJTF low-$\delta^{18}O$ units must have then been derived from some relatively shallow pre-existing low-$\delta^{18}O$ crustal source.

5.5. The origins of low-$\delta^{18}O$ volcanism at the J-P Desert and Bruneau–Jarbidge/Twin Falls

We have shown that the oldest known Miocene rhyolite in the vicinity of the central SRP, the Rough Mountain Rhyolite, is in fact depleted in $\delta^{18}O$, though this depletion is relatively minor relative to those of younger BJTF units (Fig. 4). This is despite the fact that $\delta^{18}O_{plag}$ values in this unit are diverse and range to very low values, because we interpret the highest single crystal $\delta^{18}O_{plag}$ values in the Rough Mountain Rhyolite and in other units as the ones most closely reflecting magmatic $\delta^{18}O$ values, as they are in equilibrium with quartz phenocrysts (which resist alteration) analyzed from the same sample. Conversely, we consider the lower $\delta^{18}O_{plag}$ values to reflect post-emplacement alteration equivalent to that required for the first stage of the caldera recycling model of low-$\delta^{18}O$ magma formation, as plagioclase is highly susceptible to resetting of its $\delta^{18}O$ value by secondary alteration (these values are dashed boxes in Figure 4 and noted in Table 1). The best evidence of early (predating any Miocene calderas) low-$\delta^{18}O$ magma formation in the region, however is the fact that zircons in the Rough Mountain Rhyolite have $\delta^{18}O$ values as low as 0.5‰ (Fig. 5, Table 2). Zircons in hydrothermally-altered rocks such as the J-P Desert rhyolites or those being formed today at Yellowstone survive hydrothermal alteration intact and retain their magmatic $\delta^{18}O$ values (e.g., Bindeman and Simakin, 2014), even when most other minerals and glass are altered to low-$\delta^{18}O$ compositions. The presence of low-$\delta^{18}O$ zircons in the J-P Desert

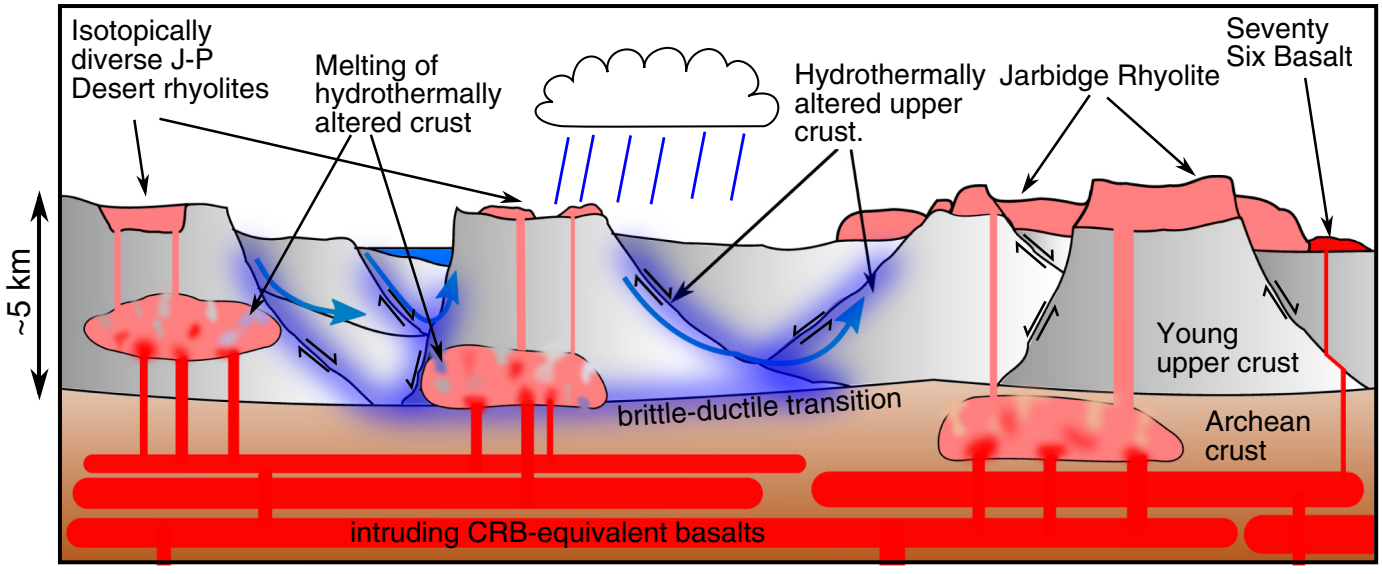

Fig. 7. Schematic sketch illustrating the model for production of low-$\delta^{18}O$ and low-ε_{Hf} rhyolites in an area of extension and plume-driven intrusion of basalt. Meteoric water (blue arrows) intrudes along normal faults, where it interacts with shallow country rocks which have ε_{Hf} of approximately zero (gray) to produce low-$\delta^{18}O$ crust (shaded blue). Meanwhile, thick basalt sills (red) accumulate in deep Archean-age crust (brown), a very small quantity of which erupts as the Seventy Six basalt. Heat from these sills drives the hydrothermal alteration of the upper crust, and is responsible for crustal melting to produce the erupted rhyolites of the Jarbidge area and the J-P Desert. The Jarbidge rhyolite erupted first, and as such is cut by systems of faults that do not cut products of younger volcanism at BJTF (and possibly also the intermediate-age J-P Desert rhyolites). In this illustration, we have shown the crust below the brittle–ductile transition as being exclusively Archean in age, and vice versa, a likely oversimplification that nonetheless explains the data well. (For interpretation of the references to color in this figure legend, the reader is referred to the web version of this article.)

rhyolites therefore allows us to confidently say that their composition reflects the composition of their parent magma, rather than post-emplacement alteration. There therefore must have been low-$\delta^{18}O$ crust present beneath the J-P Desert prior to the formation of the first Miocene rhyolites there at ~15 Ma. This allows us to discard the caldera recycling model as an explanation for the emergence of low-$\delta^{18}O$ in the neighborhood of the central SRP.

Continued widespread low-$\delta^{18}O$ volcanism in the BJTF (13–8 Ma) center after the earlier J-P Desert volcanism suggests that the low-$\delta^{18}O$ crust that melted to form the J-P Desert magmas is regionally abundant, though its identity is uncertain. One possibility is that earlier Cenozoic volcanic rocks such as the Cretaceous granitoids and Eocene volcanic and intrusive rocks which outcrop in the area (Fig. 1) underwent hydrothermal alteration coeval with their formation and later melted to form the low-$\delta^{18}O$ magmas observed in the J-P Desert and the BJTF center. This is the view advocated by Boroughs et al. (2005, 2012) and favored by Ellis et al. (2013).

We prefer another possible source of low-$\delta^{18}O$ rocks in the region: that shallow crust in the region was hydrothermally altered only shortly before the eruption of the J-P Desert rhyolites. Basin and Range faulting became active in northern Nevada at 16–15 Ma, coincident with the eruption of the CRBs (Brueseke et al., 2014; Colgan, 2013; Colgan and Henry, 2009), although the exact (i.e. within 1 Ma resolution) timing of extension will require further field work to be constrained. Extensional tectonic regimes provide numerous opportunities for meteoric water to intrude to depths as deep as the brittle–ductile transition in volumes of many km^3 (Gottardi et al., 2013; Muir-Wood and King, 1993). Geological evidence for active faulting during volcanism in the region consists of faults that cut the 15.3 Ma Jarbidge Rhyolite but do not cut the overlying 10–13 Ma Cougar Point Tuffs (Brueseke et al., 2014). This active faulting, perhaps accentuated by the stresses associated with the underplating and intrusion of the CRBs into the crust, combined with a significantly enhanced geothermal gradient (as at Yellowstone, but perhaps even more so considering the vigor of the Columbia River Basalt eruptions) to create potentially ideal conditions to extensively hydrothermally alter the shallow crust (Fig. 7). A variation of this scenario has been advocated for the production of some low-$\delta^{18}O$ rhyolites near the Picabo eruptive center (Drew et al., 2013; Konstantinou et al., 2013), through the heat and extension associated with metamorphic core complex formation. Gottardi et al. (2013) recently modeled the isotopic depletion of the crust along normal faults, showing that significant $\delta^{18}O$ depletion along these faults and the associated detachment zones at the brittle–ductile transition is possible when the permeability of these areas is high and depths are shallow. Importantly, the roughly horizontal zone of intense alteration along these detachments may also represent a significant rheological barrier to later intruding magmas, which leads to the strongest crustal melting occurring in the areas of the greatest hydrothermal alteration, favoring the production of low-$\delta^{18}O$ magmas.

Finally, combining our new data from the J-P Desert and Jarbidge rhyolites with previous studies of the BJTF, we note a general trend of decreasing magmatic $\delta^{18}O$ with time (Fig. 4). This suggests that whatever process was responsible for the lowering of the $\delta^{18}O$ values of the crustal rocks which gave rise to the J-P Desert and BJTF rhyolites was active coeval with the magmatic activity. We therefore suggest that the first low-$\delta^{18}O$ rhyolites in the J-P Desert and greater central SRP region did not inherit their low-$\delta^{18}O$ composition from pre-Miocene hydrothermal events, as suggested by Boroughs et al. (2005, 2012). Instead, hydrothermal circulation driven by the same magmatic system that produced the rhyolites altered the local crust only shortly before continued heating and magma intrusion lead to melting of the resulting low-$\delta^{18}O$ crust. This initial hydrothermal "priming" of the crust did not lead to complete oxygen isotope equilibration of the crust with meteoric water as the earliest J-P Desert rhyolites have relatively small $\delta^{18}O$ depletions relative to later BJTF rhyolites (Fig. 4). By comparison, the Jarbidge Rhyolite (at least in the area of our sample) predated most extensional faulting where it erupted, meaning the local crust was not yet altered at all. High $\delta^{18}O$ values in the Eocene Cedar Canyon Tuff (Fig. 4) further suggest that the initial crust prior to Miocene volcanism was not low-$\delta^{18}O$ in character. After the eruption of the first low-$\delta^{18}O$ rhyolites in the J-P Desert, a combination of heating and extension of the crust led to increasing $\delta^{18}O$ depletion of the shallow crust, creating the decreasing $\delta^{18}O$ trend seen in major phenocrysts in rhyolites in the region. Further stronger $\delta^{18}O$ depletions in the younger and more dramatically depleted in ^{18}O BJTF volcanic complex can then be explained by the caldera collapse and rifting burial-remelting models previously suggested to explain low-$\delta^{18}O$ rhyolites in the East Snake River Plain and Yellowstone (e.g. Bindeman and Valley, 2001; Drew et al., 2013; Watts et al., 2011). In particular, dramatic excursions towards very low-$\delta^{18}O$ values in the 11–12 Ma Cougar Point Tuffs VII and XII (Fig. 4) may be explainable by the alteration and remelting of caldera fill material that was already low-$\delta^{18}O$ because of the more regionally extensive normal fault-driven alteration that had been active since at least 15.3 Ma (Fig. 7). Our model thus calls for pre-Miocene crustal rocks to be the initial source of low-$\delta^{18}O$ rocks in the area, as in Boroughs et al. (2005, 2012), but with the significant difference that alteration of these rocks was accomplished by the extensional tectonics and the Yellowstone plume during the Miocene only shortly before the production of rhyolite. We prefer this latter model because of the observation of time-progressive depletion in $\delta^{18}O$ of the erupted magmas.

5.6. Constraining crustal melting end-members and magmatic evolution using trace elements and isotopes in zircons

We discovered considerable diversity of Hf and O isotopic compositions between individual zircons in the J-P Desert units, including what is, to our knowledge, the largest range of zircon Hf isotope compositions reported in a single eruptive unit (the Johnstons Camp Rhyolite). The J-P Desert units have disequilibrium $\Delta^{18}O$ values in zircon–zircon, zircon–quartz, and zircon–plagioclase mineral pairs, and only a few zircons are in equilibrium with melt values suggested by major phenocrysts (Figs. 4, 5). Zircon Hf isotope compositions were also out of equilibrium with each other and whole rock values. By contrast, the Jarbidge Rhyolite zircons are much less diverse in both $\delta^{18}O$ and ε_{Hf}. Some disequilibrium in O and Hf isotopes between zircon–zircon and zircon–whole rock pairs in the Jarbidge Rhyolite does exist, but to a much lesser extent than in the J-P Desert units (Fig. 5). Despite this, the zircons within each J-P Desert unit all had U–Pb ages within error of each other (Fig. 2), suggesting that they each formed during a single magmatic event. While there are no obviously xenocrystic zircons in the Jarbidge Rhyolite, the MSWD value associated with the U–Pb ages for the Jarbidge Rhyolite zircons exceeds the limits for a homogeneous population. Pending high-precision zircon geochronology by isotope dilution thermal ionization mass spectrometry (ID-TIMS; e.g., Wotzlaw et al., 2014), this is tentatively interpreted to indicate the presence of possible antecrystic zircons and/or zircon crystallization over a period of a ~2 million years before erupting. Such protracted magmatic activity would agree with persistent volcanism in the vicinity of the main body of the Jarbidge rhyolite from 16.1 to 15.0 Ma (Brueseke et al., 2014).

Trace element variability in zircons of the J-P Desert and Jarbidge rhyolites is decidedly less dramatic than the diversity of isotopic compositions (Fig. 6). The range of Ti compositions in zircons from all units corresponds to magmatic temperatures of 790 °C to 925 °C (Ferry and Watson, 2007), assuming a Ti activity of 0.5 for all units, analogous to measured values for similarly hot hotspot rhyolites at Heise and Yellowstone (Rivera et al., 2014; Watts et al., 2011), because titanium–iron oxide compositions are almost certainly compromised by secondary alteration. Variations between units are insignificant and correlations between Ti-in-zircon and hafnium or oxygen isotopic compositions are absent. Due to significant alkali loss and secondary silicification in the J-P Desert and Jarbidge rhyolites (Bernt and Bonnichsen, 1982) we

were unable to reliably determine zircon saturation temperatures for the studied units. The Jarbidge Rhyolite zircons show a slightly stronger negative Eu anomaly than the J-P Desert units (Fig. 6), but no relationship between the Hf isotope composition of the zircons and the magnitude of the Eu or Ce anomalies was otherwise found. As observed above, we note correlations between Hf isotope composition and Nb/U and Nb/Th ratios, which likely reflects the age of crust that melted to form the initial magmas (Collerson and Kamber, 1999). Finally, a weak correlation exists between the steepness of the heavy rare earth element curve (expressed in Fig. 6 by the Yb/Gd ratio) and the ε_{Hf} value of the zircons in the Jarbidge and J-P Desert units (Fig. 6). We propose that this also reflects subtle differences in the source rocks of different ages that may prove useful in further constraining the identity of the crustal end-members that melted to produce these rhyolites (see below).

The diversity of the isotopic and trace element compositions exhibited by the zircons in the J-P Desert rhyolites clearly suggests that they crystallized in separate isotopically diverse batches of magma. This has been invoked to explain a similar diversity of zircon $\delta^{18}O$ values also observed in units from the Heise (Watts et al., 2011), Picabo (Drew et al., 2013), Yellowstone, and elsewhere (Bindeman and Simakin, 2014) centers (Fig. 1a), along the SRP track. Miocene zircon U–Pb crystallization ages and a lack of evidence of inheritance of Archean or Eocene-age zircons (Fig. 2) implies that any crust that melted to form these magmas must have been heated above zircon saturation temperatures, resorbing any pre-existing zircons into the melt (excluding the possibility that source rocks were all zircon-free, which we view as unlikely given their apparent compositional diversity). These batches then crystallized new zircons that recorded the Hf isotope compositions of the parent melt, because Hf is very compatible in zircon, but recorded new U–Pb ages, because Pb is very incompatible in zircon. The subsequent thermal and crystallization histories of these batches is less known, but must have mingled together to form the final melt which erupted and cooled before the zircons could equilibrate with each other and their host melt (e.g. Watts et al., 2011; Wotzlaw et al., 2014). This could have been accomplished by continued addition of heat causing the magma bodies to grow and merge, or perhaps via the formation of dikes or sills that connected the disparate batches of magma. Mixing of at least as many separate initial magma batches as there are distinguishable groups of zircon compositions (shaded in Fig. 5) is required to account for the spread of zircon compositions observed. Such batch assembly is common in the record of the Snake River Plain, and has also been observed at every major eruptive center in the Snake River Plain in either zircons or major phenocrysts (Bindeman and Simakin, 2014; Drew et al., 2013; Ellis and Wolff, 2012; Watts et al., 2011, 2012).

The observed heterogeneity of the zircons in the studied rhyolites suggests that the individual magma batches were derived from melting of at least two continental crust end-members with different Hf and O isotopic compositions followed by mixing with variable amounts of rhyolitic differentiates of mantle-derived basalts. This $\delta^{18}O$-ε_{Hf} relationship is in contrast to systems with variable O isotopes but homogeneous Hf (e.g. the Picabo volcanic field, Drew et al., 2013) which have been explained as the product of melting variably hydrothermally altered crust of pre-homogenized ε_{Hf} composition. The hypothesized crustal end members are: (1) Archean crust that has not experienced high-temperature hydrothermal alteration in the presence of meteoric water, with $\delta^{18}O_{qz} \approx 8‰$ and $\varepsilon_{Hf} \approx -60$ (the crustal xenolith average of Watts et al., 2010), and (2) higher-ε_{Hf} (≈ 0) and low-$\delta^{18}O$ ($\approx -1‰$) crust which we identify as much younger rocks that have experienced shallow hydrothermal alteration by meteoric water shortly prior to rhyolite production, as is discussed above. Potential candidates for crustal end member (2) are Eocene volcanic rocks and Cretaceous granitoids exposed at the surface in the J-P Desert area (Fig. 1). We hypothesize remelting of these Eocene volcanic rocks and Cretaceous granitoids to create the Miocene-age, low-$\delta^{18}O$ magmas and zircons observed in the J-P Desert units (Fig. 7). If we take the lowest $\delta^{18}O$ and highest ε_{Hf} zircons as indicative of the approximate composition of end member (2), we estimate that it has $\varepsilon_{Hf} \approx \varepsilon_{Nd} \approx 0$ and $\delta^{18}O \approx 0‰$. All zircon compositions for the rhyolites studied here fall between these two crustal end-member compositions and a third, mantle-like composition with a $\delta^{18}O$ of $+6‰$ and an ε_{Hf} value of roughly 0 (Fig. 5). This component is most likely a rhyolitic differentiate of intruding CRBs, which also provided the heat for melting of the crustal end-members. Notably, the Archean crustal end-member seems to have escaped any hydrothermal alteration. We suggest that this simply means that the Archean rocks that melted to form the Miocene magmas were physically removed from the zones of hydrothermal alteration, perhaps by being deeper (Fig. 7), though we concede that this could be interpreted to support the model of Boroughs et al. (2012) which suggests that the low-$\delta^{18}O$ crust in the region has pre-Miocene age and also acquired its isotopic composition in a separate hydrothermal event coeval with their formation.

Among the zircon compositions observed in the J-P Desert and Jarbidge rhyolites, only a few appear to be derived from nearly pure crustal melts, and while many are derived significantly more from crustal melt than mantle differentiate, and no zircons record the composition of pure uncontaminated mantle differentiates (Fig. 5). This is actually unsurprising as the introduction of large volumes of hot intrusive mantle magmas should cause significant melting of the surrounding silicic crust (Annen et al., 2006; Dufek and Bergantz, 2005; Huppert and Sparks, 1988), and the resulting contrasting silicic melts derived from the mantle and the crust should then rapidly mix. The process that creates the final hybrid magma must fall between two end-member scenarios: 1) mafic magma melts the surrounding crust in an approximately one-to-one ratio, producing batch melts of an intermediate composition which then differentiate to rhyolite, 2) mafic magma provides heat for crustal melting but differentiates into a more silicic composition in isolation; this differentiate is hotter than the crustal melt and remains zircon-undersaturated, and once it reaches rhyolitic composition it mixes with the crustal melts (Simakin and Bindeman, 2012). Supporting scenario 2 is Fig. 5, which illustrates that the majority of zircons in the Rough Mountain Rhyolite and the Lapilli Tuff of Sheep Creek are lower in $\delta^{18}O$ than equilibrium zircon values of ~3.3‰ predicted by major phenocrysts, which best represent the composition of the final erupted magma. This suggests that a zircon-undersaturated normal-

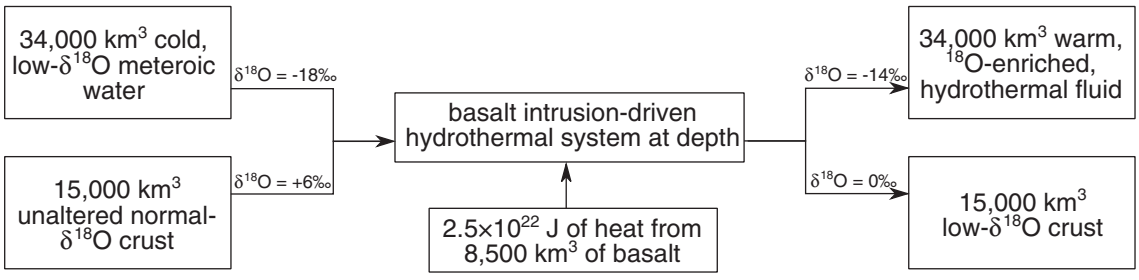

Fig. 8. Block diagram showing the requirements of meteoric water and intruding basalt to hydrothermally alter 15,000 km^3 of shallow crust in the central SRP to provide a source for the widespread low-$\delta^{18}O$ volcanism that occurred there.

$\delta^{18}O$ melt mixed with the zircon-bearing, low-$\delta^{18}O$ crustal melts, raising the $\delta^{18}O$ value of the whole mix without contributing high-$\delta^{18}O$ zircons (Fig. 5). This magma crystallized quartz whose isotopic composition reflects the new bulk magma $\delta^{18}O$ value, but few to no new zircons, suggesting that eruption was very rapid after this final mixing event. The zircon-undersaturated magma was also likely rhyolitic as a more mafic magma would have dissolved the pre-existing zircons in the mixing event. We suggest that this magma is a hot differentiate of the intruding basalts, with relatively minor crustal contamination, as in scenario 2. The average composition of erupted CRB magmas is also basaltic andesite, rather than primitive basalt (Hooper and Hawkesworth, 1993); if that composition is primary, it markedly reduces the amount of initial intrusive material needed to produce rhyolitic differentiates via fractional crystallization prior to mixing with crustal melts. Finally, the relative lack of zircons with compositions mirroring the whole-rock compositions of the Rough Mountain and Johnstons Camp Rhyolites suggests that eruption occurred rapidly after assembly, before additional new zircons could form in the final melt, further suggesting that the assembly process may quickly lead to the eruption of the final mingled melt.

5.7. Total basaltic input into the crust

High-temperature hydrothermal alteration of the crust, the production of crustal partial melts with rhyolitic composition, and the production of isotopically mantle-like rhyolites via fractional crystallization of basaltic magma indirectly and directly require input of basalt into the crust, either as a heat source or as a direct source of material. The total volume of rhyolite erupted in the central SRP and the Jarbidge Mountains during the mid-Miocene, nearly all of which is low-$\delta^{18}O$, was at least 10,000 km^3 (Bonnichsen et al., 2008). We estimate that to produce these rhyolites, subequal volumes of crustal melts and rhyolitic differentiates of mantle-derived basalts are required, in line with our calculations concerning the J-P Desert rhyolites (Fig. 5), and with a similar ratio of crustal to mantle input for SRP rhyolites of up to 0.4 determined by McCurry and Rodgers (2009). Under these conditions, the addition of ~14 km thick mid-crustal sills of gabbro derived from the mantle are required underneath the entire Snake River Plain to account for the basalt needed for fractionation (McCurry and Rodgers, 2009), a suggestion borne out by geophysical observations (Peng and Humphreys, 1998; Rodgers and McCurry, 2009).

Here, we add new constraints on the amount of basalt based on our model of abundant low-$\delta^{18}O$ magmatism that results from extensive hydrothermal alteration of pre-existing crust: 1 kg of basalt cooling from 1200 °C to 500 °C provides 1.1 MJ (cumulate heat content including latent heat of crystallization, based on a specific heat of 1.34 J/g and a latent heat of crystallization of 418 J/g, Huppert and Sparks, 1988) is necessary to raise the temperature of 1.5 kg of meteoric water from 25 °C to 200 °C. If we take 4‰ as the typical $\delta^{18}O$ enrichment of a 200 °C hydrothermal fluid after water–rock interaction, such as in Yellowstone's Upper Geyser Basin (Fournier, 1989; Hurwitz et al., 2012), and assume a 6‰ $\delta^{18}O$ depletion of the crustal rock over the duration of the alteration episode (the full range of zircon diversity we observe, Figs. 5, 6), we arrive at a water/rock ratio of 1.5. This is equivalent to a basalt/altered shallow crust volume ratio of approximately 0.55, suggesting that to alter 15,000 km^3 of crust in the central SRP (which we consider to be conservative given the 10,000 km^3 of low-$\delta^{18}O$ rhyolite), some 8200 km^3 of basalt must have intruded and solidified to provide the necessary heat (Fig. 8). This figure is supported by earlier thermal estimates in Taylor (1974), who suggested that to an order of magnitude approximation, hydrothermal alteration of a certain volume of shallow crust requires thermal input from a similar volume of intruded magma. This number is not implausible if one takes into account that this intrusion may have occurred gradually over 3.5 Ma from the start of CRB eruptions to the start of BJTF eruptions, equivalent to an influx of only 0.002 km^3/yr on average. Much larger fluxes of intruding basalt are suggested for Yellowstone today, and Fournier (1989) suggests that 0.08 km^3 per year of basalt is needed to drive the present hydrothermal system at Yellowstone, suggesting that the process of alteration of the crust is not efficient in terms of heat transferred from basalt to water altering new crust. If we estimate the area underlain by these basalt intrusions to be 120 km by 120 km (14,400 km^2), the required basaltic sill complex to drive all of the observed hydrothermal alteration need not be more than approximately 0.6 km thick to account for the calculated 8500 km^3 of intruded basalt. In comparison to the ~15 km thickness of basaltic intrusions required by other studies (e.g. Leeman et al., 2008; McCurry and Rodgers, 2009) needed to account for the physical production of the erupted rhyolites by melting and fractionation, this number represents a small fraction of the total available basalt (and therefore heat) available in the system. It is thus easily plausible, and perhaps inescapable, for the voluminous syn-volcanic hydrothermal alteration that we propose for the BJTF system in general to be accomplished by excess intruded basalts in the overall system.

6. Conclusion

We present a detailed study of the first rhyolites to erupt in the neighborhood of the central Snake River Plain in the Miocene. These early rhyolites include voluminous low-$\delta^{18}O$ (but not so low as the main phase Bruneau–Jarbidge magmas) rhyolitic magmas with diverse ε_{Hf} and ε_{Nd} which erupted southwest of the Bruneau–Jarbidge volcanic center at ~15 Ma, coeval with the termination of the main phase of CRB eruptions. These early silicic eruptions derived their oxygen, hafnium, and neodymium isotopic compositions from 1) Archean crust, characterized by normal oxygen isotopes and extremely unradiogenic Hf and Nd isotopes, and 2) younger hydrothermally altered silicic crustal crust with more radiogenic Hf and Nd, which is likely equivalent to Eocene volcanic and subvolcanic intrusive rocks or Cretaceous intrusions outcropping in the area. U–Pb crystallization ages of zircons from these units are with a few exceptions indistinguishable from the inferred eruption ages given by the youngest zircon ages, and xenocrystic zircons are entirely absent. These zircons, however, show remarkable diversity in $\delta^{18}O$ (−0.6‰ to +6.5‰) and ε_{Hf} (−39 to −1), suggesting that these magmas were assembled in the shallow crust from many batches of compositionally distinct magma derived from mixtures of melts of the above two crustal-end members and a mantle-derived component. The lowering of magmatic $\delta^{18}O$ values from the oldest J-P Desert rhyolites the younger Bruneau–Jarbidge rhyolites is a result of the remelting of crust that was being hydrothermally altered coeval with rhyolite production. This hydrothermal alteration was most likely driven by a combination of normal faulting, which provides pathways for meteoric water to penetrate the shallow crust, and increased geothermal gradients caused by voluminous intrusions of the basalt similar to the main phase Columbia River Basalt erupted lavas. These basaltic intrusions were also responsible for local rhyolite production by providing a heat source for crustal melting and by fractional crystallization. We suggest that this mantle plume-induced hydrothermal alteration and later crustal melting may characterize other areas of intraplate volcanism in an extensional environment.

Acknowledgments

We thank Jim Palandri for his help in the stable isotope lab, Jade Star Lakey for XRF work on the Jarbidge rhyolite, and Bill Bonnichsen for providing a sample of the Jarbidge Rhyolite. This work was supported by NSF grant EAR/CAREER0844772, and the ion microprobe facility at UCLA utilized during this study is partly supported by grant 1029193 from the Instrumentation and Facilities Program, Division of Earth Sciences, National Science Foundation.

Appendix A. Supplementary data

Supplementary data to this article can be found online at http://dx.doi.org/10.1016/j.lithos.2015.02.022. This includes detailed information on sample locations and stratigraphy, and all analyses of major elements, trace elements, and isotopes made of whole rocks, major phenocrysts, and zircons for this study.

References

Annen, C., Blundy, J.D., Sparks, R.S.J., 2006. The genesis of intermediate and silicic magmas in deep crustal hot zones. Journal of Petrology 47 (3), 505–539.

Arndt, N.T., Goldstein, S.L., 1987. Use and abuse of crust-formation ages. Geology 15 (10), 893–895.

Belousova, E.A., Griffin, W.L., O'Reilly, S.Y., Fisher, N.I., 2002. Igneous zircon: trace element composition as an indicator of source rock type. Contributions to Mineralogy and Petrology 143, 602–622.

Berglund, M., Weiser, M.E., 2011. Isotopic compositions of the elements 2009 (IUPAC Technical Report). Pure and Applied Chemistry 83 (2), 397–410.

Bernt, J., Bonnichsen, B., 1982. Pre-Cougar Point Tuff Volcanic Rocks Near the Idaho-Nevada Border, Owyhee County, Idaho. In: Bonnichsen, B., Breckenridge, R.M. (Eds.), Cenozoic geology of Idaho. Idaho Bureau of Mines and Geology Bulletin 26, pp. 321–330.

Bindeman, I.N., 2008. Oxygen isotopes in mantle and crustal magmas as revealed by single crystal analysis. Reviews in Mineralogy and Geochemistry 69, 445–478.

Bindeman, I.N., Simakin, A.G., 2014. Rhyolites—hard to produce but easy to recycle and sequester: integrating microgeochemical observations and numerical models. Geosphere 10 (5), 930–957.

Bindeman, I.N., Valley, J., 2001. Low-$\delta^{18}O$ rhyolites from Yellowstone: magmatic evolution based on analyses of zircons and individual phenocrysts. Journal of Petrology 42 (8), 1491–1517.

Bindeman, I.N., 2003. Crystal sizes in evolving silicic magma chambers. Geology 31 (4), 367–370.

Bonnichsen, B., Leeman, W.P., Honjo, N., McIntosh, W.C., Godchaux, M.M., 2008. Miocene silicic volcanism in southwestern Idaho: geochronology, geochemistry, and evolution of the central Snake River Plain. Bulletin of Volcanology 70, 315–342.

Boroughs, S., Wolff, J., Bonnichsen, B., Godchaux, M., Larson, P., 2005. Large-volume, low-$\delta^{18}O$ rhyolites of the Central Snake River Plain, Idaho, USA. Geology 33, 821–824.

Boroughs, S., Wolff, J.A., Ellis, B.S., Bonnichsen, B., Larson, P.B., 2012. Evaluation of models for the origin of low-$\delta^{18}O$ rhyolites of the Yellowstone/Columbia River Large Igneous Province. Earth and Planetary Science Letters 313–314, 45–55.

Bouvier, A., Vervoort, J.D., Patchett, P.J., 2008. The Lu–Hf and Sm–Nd isotopic composition of CHUR: constraints from unequilibrated chondrites and implications for the bulk composition of terrestrial planets. Earth and Planetary Science Letters 273, 48–57.

Branney, M.J., Bonnichsen, B., Andrews, G.D.M., Ellis, B., Barry, T.L., McCurry, M., 2008. 'Snake River (SR)-type' volcanism at the Yellowstone hotspot track: distinctive products from unusual, high-temperature silicic super-eruptions. Bulletin of Volcanology 70, 293–314.

Brueseke, M.E., Callicoat, J.S., Hames, W., Larson, P.B., 2014. Mid-Miocene rhyolite volcanism in northeastern Nevada: the Jarbidge Rhyolite and its relationship to the Cenozoic evolution of the northern Great Basin (U.S.A.). Geological Society of America Bulletin 126 (7-8) (B30736.1).

Burov, E., Guillou-Frottier, L., 2005. The plume head-continental lithosphere interaction using a tectonically realistic formulation for the lithosphere. Geophysical Journal International 161 (2), 469–490.

Callicoat, J.S., 2010. Significance of mid-Miocene volcanism in northeast Nevada: Petrographic, Chemical, Isotopic, and Temporal Importance of the Jarbidge Rhyolite. Kansas State University (M.S. Thesis).

Camp, V.E., Ross, M.E., 2004. Mantle dynamics and genesis of mafic volcanism in the intermontane Pacific Northwest. Journal of Geophysical Research 109, B08204.

Camp, V.E., Ross, M.E., Duncan, R.A., Jarboe, N.A., Coe, R.S., Hanan, B.B., Johnson, J.A., 2013. The Steens Basalt: earliest lavas of the Columbia River Basalt Group. In: Reidel, S.P., Camp, V.E., Ross, M.E., Wolff, J.A., Martin, B.S., Tolan, T.L., Wells, R.E. (Eds.), Geological Society of America Special Paper 497, pp. 87–116.

Carlson, R., 1984. Isotopic constraints on Columbia River flood basalt genesis and the nature of the subcontinental mantle. Geochimica et Cosmochimica Acta 48 (11), 2357–2372.

Chiba, H., Chacko, T., Clayton, R.N., Goldsmith, J.R., 1989. Oxygen isotope fractionations involving diopside, forsterite, magnetite, and calcite: Application to geothermometry. Geochimica et Cosmochimica Acta 53, 2985–2995.

Christiansen, E.H., Foulger, G.R., Evans, J.R., 2002. Upper-mantle origin of the Yellowstone hotspot. Geological Society of America Bulletin 114 (10), 1245–1256.

Coats, R.R., 1987. Geology of Elko County. Nevada Bureau of Mines and Geology Bulletin, Nevada, p. 101.

Coble, M.A., Mahood, G.A., 2012. Initial impingement of the Yellowstone plume located by widespread silicic volcanism contemporaneous with Columbia River flood basalts. Geology 40, 655–658.

Colgan, J.P., 2013. Reappraisal of the relationship between the northern Nevada rift and Miocene extension in the northern Basin and Range Province. Geology 41, 211–214.

Colgan, J.P., Henry, C.D., 2009. Rapid middle Miocene collapse of the Mesozoic orogenic plateau in north-central Nevada. International Geology Review 51 (9–11), 920–961.

Collerson, K.D., Kamber, B.S., 1999. Evolution of the continents and the atmosphere inferred from Th–U–Nb systematics of the depleted mantle. Science 283, 1519–1522.

Cummings, M.L., Evans, J.G., Ferns, M.L., Lees, K.R., 2000. Stratigraphic and structural evolution of the middle-Miocene synvolcanic Oregon-Idaho graben. Geological Society of America Bulletin 112 (5), 668–682.

DePaolo, D.J., 1981. Neodymium isotopes in the Colorado Front Range and crust–mantle evolution in the Proterozoic. Nature 291, 193–196.

Doe, B.R., Leeman, W.P., Christiansen, R.L., Hedge, C.E., 1982. Lead and strontium isotopes and related trace elements as genetic tracers in the upper Cenozoic rhyolite–basalt association of the Yellowstone Plateau volcanic field. Journal of Geophysical Research 87, 4785–4806.

Drew, D.L., Bindeman, I.N., Watts, K.E., Schmitt, A.K., Fu, B., McCurry, M., 2013. Crustal-scale recycling in calderas and rift zones along the Yellowstone hotspot track: O and Hf isotopic evidence in diverse zircons from voluminous rhyolites of the Picabo volcanic field, Idaho. Earth and Planetary Science Letters 381, 63–77.

Dufek, J., Bergantz, G.W., 2005. Lower crustal magma genesis and preservation: a stochastic framework for the evaluation of basalt–crust interaction. Journal of Petrology 46 (11), 2167–2195.

Ellis, B.S., Wolff, J.A., 2012. Complex storage of rhyolite in the central Snake River Plain. Journal of Volcanology and Geothermal Research 211–212, 1–11.

Ellis, B.S., Wolff, J.A., Boroughs, S., Mark, D.F., Starkel, W.A., Bonnichsen, B., 2013. Rhyolitic volcanism of the central Snake River Plain: a review. Bulletin of Volcanology 75 (745).

Ferns, M.L., McClaughry, J.D., 2013. Stratigraphy and volcanic evolution of the middle Miocene to Pliocene La Grande–Owyhee eruptive axis in eastern Oregon. In: Reidel, S.P., Camp, V.E., Ross, M.E., Wolff, J.A., Martin, B.S., Tolan, T.L., Wells, R.E. (Eds.), Geological Society of America Special Paper 497, pp. 401–427.

Ferry, J.M., Watson, E.B., 2007. New thermodynamic models and revised calibrations for Ti-in-zircon and Zr-in-rutile thermometers. Contributions to Mineralogy and Petrology 154, 429–437.

Fisher, C.M., Vervoort, J.D., DuFrane, S.A., 2014. Accurate Hf isotope determinations of complex zircons using the "laser ablation split stream" method. Geochemistry, Geophysics, Geosystems 15 (1).

Foster, D.A., Mueller, P.A., Mogk, D.W., Wooden, J.L., Vogl, J.J., 2006. Proterozoic evolution of the western margin of the Wyoming craton: implications for the tectonic and magmatic evolution of the northern Rocky Mountains. Canadian Journal of Earth Sciences 43, 1601–1619.

Fournier, R.O., 1989. Geochemistry and dynamics of the Yellowstone National Park hydrothermal system. Annual Review of Earth and Planetary Sciences 17, 13–53.

Gans, P.B., 1987. An open-system, two-layer crustal stretching model for the eastern Great Basin. Tectonics 6 (1), 1–12.

Gaschnig, R.M., Vervoort, J.D., Lewis, R.S., Tikoff, B., 2011. Isotopic evolution of the Idaho Batholith and Challis Intrusive Province, Northern US Cordillera. Journal of Petrology 52 (12), 2397–2429.

Global Multi-Resolution Topography (GMRT) synthesis. Geomappapp.org.

Gottardi, R., Kao, P., Saar, M.O., Teyssier, C., 2013. Effects of permeability fields on fluid, heat, and oxygen isotope transport in extensional detachment systems. Geochemistry, Geophysics, Geosystems 14 (5), 1493–1522.

Guillong, M., Meier, D.L., Allan, M.M., Heinrich, C.A., Yardley, B.W.D., 2008. SILLS: a MATLAB-based program for the reduction of laser ablation ICP-MS data of homogeneous material and inclusions. Mineralogical Association of Canada Short Course 40, 328–333.

Hart, W.K., Carlson, R.W., 1985. Distribution and geochronology of Steens Mountain-type basalts from the northwestern Great Basin. Isochron/West 43, 5–10.

Hooper, P., Hawkesworth, C., 1993. Isotopic and geochemical constraints on the origin and evolution of the Columbia River Basalt. Journal of Petrology 34 (6), 1203–1246.

Huppert, H.E., Sparks, R.S.J., 1988. The generation of granitic magmas by intrusion of basalt into continental crust. Journal of Petrology 29 (3), 599–624.

Hurwitz, S., Hung, A.G., Evans, W.C., 2012. Temporal variations of geyser water chemistry in the Upper Geyser Basin, Yellowstone National Park, USA. Geochemistry, Geophysics, Geosystems 13 (12).

Konstantinou, A., Valley, J., Strickland, A., Miller, E.L., Fisher, C., Vervoort, J., Wooden, J., 2013. Geochemistry and geochronology of the Jim Sage volcanic suite, southern Idaho: implications for Snake River Plain magmatism and its role in the history of Basin and Range extension. Geosphere 9 (6).

Leeman, W.P., Annen, C., Dufek, J., 2008. Snake River Plain—Yellowstone silicic volcanism: implications for magma genesis and magma fluxes. Geological Society of London, Special Publication 304, 235–259.

Link, P.K., 2002. Owyhee County, Idaho. Digital Atlas of Idaho.

Liu, L., Stegman, D.R., 2012. Origin of Columbia River flood basalt controlled by propagating rupture of the Farallon slab. Nature 482, 386–389.

Mahon, K.I., 1996. The New "York" regression: application of an improved statistical method to geochemistry. International Geology Review 38 (4), 293–303.

McCurry, M., Rodgers, D.W., 2009. Mass transfer along the Yellowstone hotspot track I: petrologic constraints on the volume of mantle-derived magma. Journal of Volcanology and Geothermal Research 188, 86–98.

McDonough, W.F., Sun, S.-s., 1995. The composition of the Earth. Chemical Geology 120, 223–253.

Menzies, C.D., Teagle, D.A., Craw, D., Cox, S.C., Boyce, A.J., Barrie, C.D., Roberts, S., 2014. Incursion of meteoric waters into the ductile regime in an active orogen. Earth and Planetary Science Letters 399, 1–13.

Milisenda, C.C., Liew, T.C., Hofmann, A.W., Kröner, A., 1988. Isotopic mapping of age provinces in Precambrian high-grade terrains: Sri-Lanka. The Journal of Geology 96 (5), 608–615.

Muir-Wood, R., King, G.C.P., 1993. Hydrological signatures of earthquake strain. Journal of Geophysical Research 98 (B12), 22,035–22,068.

Nash, B.P., Perkins, M.E., Christensen, J.N., Lee, D., Halliday, A.N., 2006. The Yellowstone hotspot in space and time: Nd and Hf isotopes in silicic magmas. Earth and Planetary Science Letters 247, 143–156.

Norman, M.D., Mertzman, S.A., 1991. Petrogenesis of Challis volcanics from central and southwestern Idaho: trace element and Pb isotopic evidence. Journal of Geophysical Research 96 (B8), 13279–13293.
Paces, J.B., Miller, J.D., 1993. Precise U–Pb ages of Duluth Complex and related mafic intrusions, Northeastern Minnesota: geochronological insights to physical, petrogenetic, paleomagnetic, and tectonomagmatic processes associated with the 1.1 Ga midcontinent rift system. Journal of Geophysical Research 98 (B8), 13997–14013.
Peng, X., Humphreys, E.D., 1998. Crustal velocity structure across the eastern Snake River Plain and the Yellowstone swell. Journal of Geophysical Research 103 (B4), 7171–7186.
Pierce, K.L., Morgan, L.A., 1992. The track of the Yellowstone hotspot: volcanism, faulting, and uplift. Geological Society of America Memoirs 179, 1–54.
Rahl, J.M., Foland, K.A., McGrew, A.J., 2002. Transition from contraction to extension in the northeastern Basin and Range: new evidence from the Copper Mountains, Nevada. Journal of Geology 110, 179–194.
Reidel, S.P., Camp, V.E., Tolan, T.L., Martin, B.S., 2013. The Columbia River flood basalt province: stratigraphy, areal extent, volume, and physical volcanology. In: Reidel, S.P., Camp, V.E., Ross, M.E., Wolff, J.A., Martin, B.S., Tolan, T.L., Wells, R.E. (Eds.), Geological Society of America Special Paper 497, pp. 1–43.
Rivera, T.A., Schmitz, M.D., Crowley, J.L., Storey, M., 2014. Rapid magma evolution constrained by zircon petrochronology and $^{40}Ar/^{39}Ar$ sanidine ages for the Huckleberry Ridge Tuff, Yellowstone, USA. Geology 42, 643–646.
Rodgers, D.W., McCurry, M., 2009. Mass transfer along the Yellowstone hotspot track II: kinematic constraints on the volume of mantle-derived magma. Journal of Volcanology and Geothermal Research 188, 99–107.
Schmandt, B., Dueker, K., Humphreys, E., Hansen, S., 2012. Hot mantle upwelling across the 660 beneath Yellowstone. Earth and Planetary Science Letters 331–332, 224–236.
Simakin, A.G., Bindeman, I.N., 2012. Remelting in caldera and rift environments and the genesis of hot, "recycled" rhyolites. Earth and Planetary Science Letters 337, 224–235.
Sláma, J., Košler, J., Condon, D.J., Crowley, J.L., Gerdes, A., Hanchar, J.M., Horstwood, M.S.A., Morris, G.A., Nasdala, L., Norberg, N., Schaltegger, U., Schoene, B., Tubrett, M.N., Whitehouse, M.J., 2008. Plešovice zircon—a new natural reverence material for U–Pb and Hf isotopic microanalysis. Chemical Geology 249 (1–2), 1–35.
Söderlund, U., Patchett, P.J., Vervoort, J.D., Isachsen, C.E., 2004. The ^{176}Lu decay constant determined by Lu–Hf and U–Pb isotope systematics of Precambrian mafic intrusions. Earth and Planetary Science Letters 219, 311–324.
Steiner, A., Streck, M.J., 2013. The Strawberry Volcanics: generation of 'orogenic' andesites from tholeiite within and intra-continental volcanic suite centered on the Columbia River flood basalt province, USA. Geological Society of London, Special Publication 385, 281–302.
Streck, M.J., Ferns, M.L., Ricker, C., Steiner, A., 2011. The Dinner Creek Tuff and other Mid-Miocene rhyolites at the magmatic focal zone of the Columbia River Basalt Group. Abs. Geological Society of America Rocky Mountain and Cordilleran Joint Meeting. 2011, pp. 3–5.
Taylor, H.P., 1974. The Application of Oxygen and Hydrogen Isotope Studies to Problems of Hydrothermal Alteration and Ore Deposition. Economic Geology 69, 843–883.
Trail, D., Mojzsis, S.J., Harrison, T.M., Schmitt, A.K., Watson, E.B., Young, E.D., 2007. Constraints on Hadean zircon protoliths from oxygen isotopes, Ti-thermometry, and rare earth elements. Geochemistry, Geophysics, Geosystems 8 (6).
Valley, J.W., Kitchen, N., Kohn, M.J., Niendorf, C.R., Spicuzza, M.J., 1995. UWG-2, a garnet standard for oxygen isotope ratios: strategies for high precision and accuracy with laser heating. Geochimica et Cosmochimica Acta 59 (24), 5223–5231.
Watts, K.E., Leeman, W.P., Bindeman, I.N., Larson, P.B., 2010. Supereruptions of the Snake River Plain: two-stage derivation of low-$\delta^{18}O$ rhyolites from normal-$\delta^{18}O$ crust as constrained by Archean xenoliths. Geology 38, 503–506.
Watts, K.E., Bindeman, I.N., Schmitt, A.K., 2011. Large-volume rhyolite genesis in Caldera Complexes of the Snake River Plain: insights from the Kilgore Tuff of the Heise Volcanic Field, with comparison to Yellowstone and Bruneau–Jarbidge Rhyolites. Journal of Petrology 52 (5), 857–890.
Watts, K.E., Bindeman, I.N., Schmitt, A.K., 2012. Crystal scale anatomy of a dying supervolcano: and isotope and geochronology study of individual phenocrysts from voluminous rhyolites of the Yellowstone caldera. Contributions to Mineralogy and Petrology 164 (1), 45–67.
Wiedenbeck, M., Hanchar, J.M., Peck, W.H., Sylvester, P., Valley, J., Whitehouse, M., Kronz, A., Morishita, Y., Nasdala, L., Fiebig, J., Franchi, I., Girard, J.P., Greenwood, R.C., Hinton, R., Kita, N., Manson, P.R.D., Norman, M., Ogasawara, M., Piccoli, R., Rhede, D., Satoh, H., Schulz-Dobrick, B., Skar, O., Spicuzza, M.J., Terada, K., Tindle, A., Togashi, S., Vennemann, T., Xie, Q., Zheng, Y.F., 2004. Further characterization of the 91500 zircon crystal. Geostandards and Geoanalytical Research 28, 9–39.
Wolff, J.A., Ramos, F.C., Hart, G.L., Patterson, J.D., Brandon, A.D., 2008. Columbia River flood basalts from a centralized crustal magmatic system. Nature Geoscience 1, 177–180.
Wotzlaw, J.F., Bindeman, I.N., Watts, K.E., Schmitt, A.K., Caricchi, L., Schaltegger, U., 2014. Linking rapid magma reservoir assembly and eruption trigger mechanisms at evolved Yellowstone-type supervolcanoes. Geology 42 (9), 807–810.